8-1995

Preprocessing of microcirculatory images.

Mohamed S. Mansour
University of Louisville

PREPROCESSING OF MICROCIRCULATORY IMAGES

By

Mohamed S. Mansour
B.Sc., Ain Shams University. 1991

A Thesis
Submitted to the Faculty of the
Graduate School of the University of Louisville
in Partial Fulfillment of the Requirements
for the Degree of

MASTER OF SCIENCE

Department of Engineering Mathematics and Computer Science

August 1995

ABSTRACT

This thesis project consists of the development of a computerized image processing system to preprocess microvascular images of the mouse Latisimus Dorsi Muscle (LDM). This research has been conducted in association with the Division of Plastic and Reconstructive Surgery at the University of Louisville. The input to the system is a set of 35 or more overlapping microscopic fields or sub_images containing segments of the LDM microcirculation, the output is an adjacent single montage encompassing the entire LDM microvasculature. The developed system presents practical solutions to the problems of image registration, overlap resolution, and image segmentation, in addition, the results of this project include simple geometrical measurements of the microvascular system such as length, tortuosity, and directionality. In future projects, the measurements should be further analyzed to study the LDM microcirculation. The entire system was written in C/C++ languages, and the Bluestone's UIM/X GUI builder. The system was implemented on the Speed School's HP–9000 Unix system. The system also takes advantage of the image processing libraries (ImageMagick) available on the system.

ACKNOWLEDGMENTS

The author would like to thank Dr. Ahmed Desoky for directing and providing instruction throughout the preparation of this thesis. Thanks are also given to Dr. John Barker for his help in writing up the introduction, Dr. Khaled Kamel for his help and support throughout the course of study, Mr. Sean Carroll and Mr. Shaad Bidiwala for their help in formulating the requirements of the system. Finally special thanks go to the author's parents Mr. Mansour and Mrs. El–Ehwany for their support.

TABLE OF CONTENTS

LIST OF FIGURES

LIST OF TABLES

CHAPTER I
INTRODUCTION

Scientists in the life sciences have studied the microcirculation for several hundred years. Some of the first published uses of a microscope were to observe these tiniest blood vessels to which they gave the name capillaries [1],[2] . At that early stage, the science of microcirculation was based on observing and describing phenomena in these small vessels. In more recent years the development of better microscope illumination and optics, and more importantly on–line methods for measuring the highly dynamic and constantly changing microcirculation has vastly advanced our understanding of this vital part of the cardiovascular system.

In the past, high magnification observation provided by a microscope was limited to viewing only one specific site in the microcirculation, (a section of arteriole, or venule or 5 to 8 capillaries at any given time). If one wishes to view other sections of the microvascular network, the microscope stage preparation must be moved to the new site leaving the original site behind. In other words two or more parts of the microcirculation cannot be viewed simultaneously. It follows that, using currently available measuring techniques, one cannot view and measure the entire microvascular network as a whole. An analogy to this is that one cannot see individual trees and the entire forest at the same time.

Traditional measurements of the microcirculation have been performed at several individual sites and based on changes at each of these, it is inferred that the entire network is changing accordingly. In many physiological circumstances in tissue, these methods suffice, however, there are some phenomenon affecting the microcirculation which change the net-

work as a whole. In these cases it impossible to infer that changes occurring at select sites describe changes of the entire network. An example of this and the reason why we developed the viewing/measuring system described herein is when a muscle is made ischemic (reduced blood flow to levels which cause metabolic and thus vascular architectural changes), hemodynamic changes cause the entire vascular network to redistribute blood flow throughout the muscle in an attempt to compensate regional decreases of blood supply.

In order to study changes in an entire microvascular network as well as at individual sites, we have developed a videomicroscopy system in which we capture adjacent high magnification fields one by one until the entire vascular network has been scanned, then these fields are pieced back together into a montage of the entire microcirculation. This system allows us to view and measure the tree and the forest simultaneously.

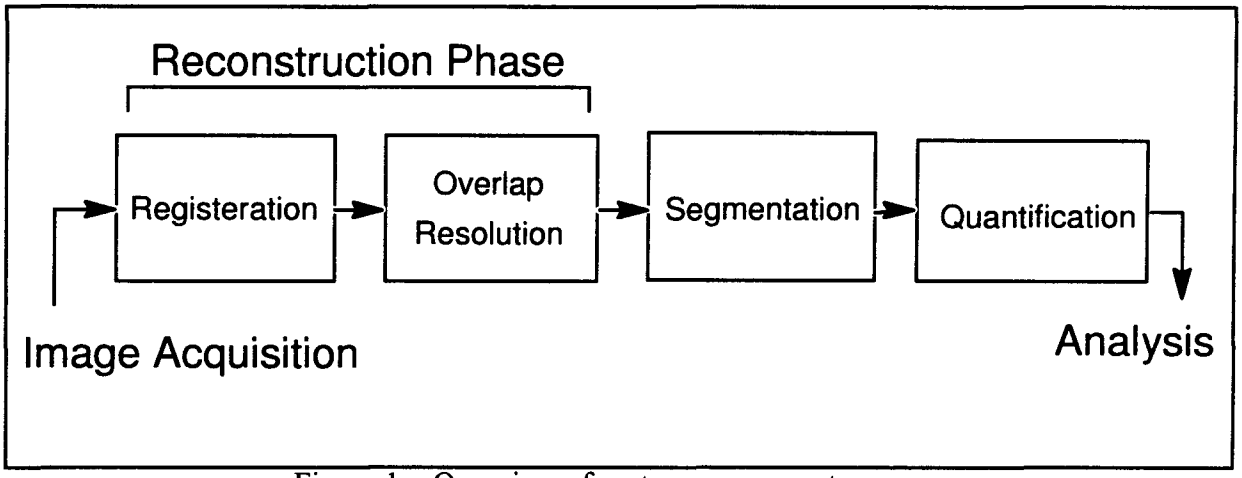

Figure 1 Overview of system components

A. Biological Methodology

The LDM of male homozygous (hr/hr) hairless mice (30–35g; 24–28 wks) was used because its vascular architecture is similar to that of humans, presenting a single neurovascular pedicle, the thoracodorsal artery, vein, and nerve (TAVN), and receiving additional blood supply from perforating vessels entering the muscle from deep (intercostal muscles) and su-

perficial (subeutaneaus tissues).. Its thin structure ($200\mu m$) permits trans– and epi–illumination and direct observation of microvasculature using video microscopy. Pentobarbital (60mg/kg; i.p.) anesthesia was used for all manipulations of the animals.

The LDM is exposed, leaving the TAVN and all the perforating vessels feeding the LDM from beneath intact. For visualization of the microcirculation, the LDM of an anesthetized mouse was gently extended over an observation platform. Mouse and platform were placed on the stage of a stereo microscope, the LDM was then epi–illuminated and viewed at X300 magnification.

B. Image Acquisition and Digitization

An FG–100 Image Processor was used for image digitization, the board was installed on a VAX–AI workstation, the resolution of the digitized images was 640x480x255. The digitized images were transferred over an Ethernet LAN to an HP–9000 workstation running HP–UX 9.01, where all subsequent image processing took place. The FG–100 board has extensive capabilities for real–time image processing, only the digitization features were use. Resolution of the digitized sub_images was 640x480x255.

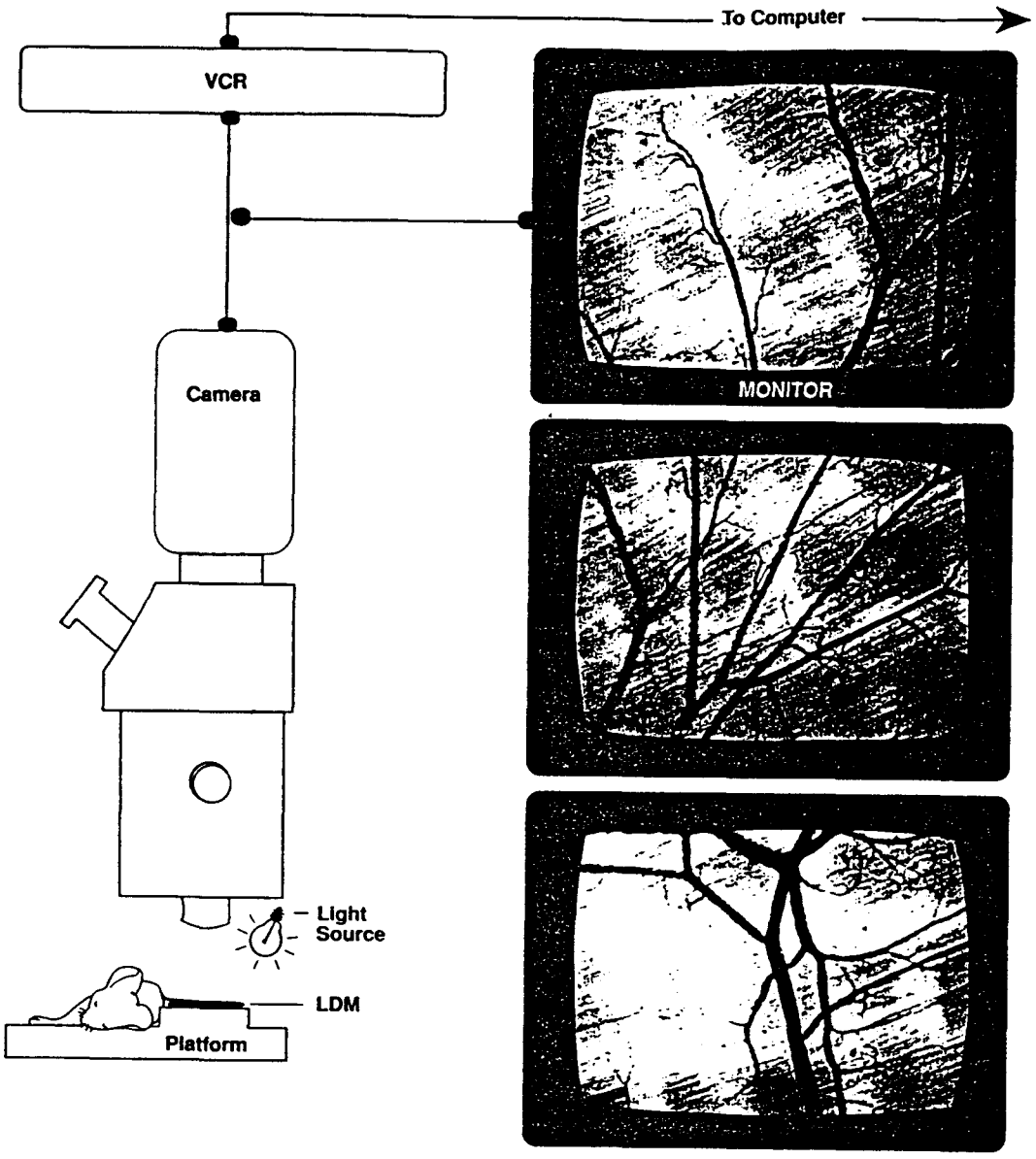

Figure 2 Video microscopy setup

C. Image Registration

The analysis of the image starts with capturing individual adjacent microscope fields of the LDM microcirculation on video tape using a microscope, camera and VCR. Later a Frame Grabber is used to capture and digitize the frames from the replayed video tape. Multi-

ple adjacent digitized sub_images make up "K" or the entire LDM microcirculation.. The resulting sub_images are of poor quality, and are highly overlapping.

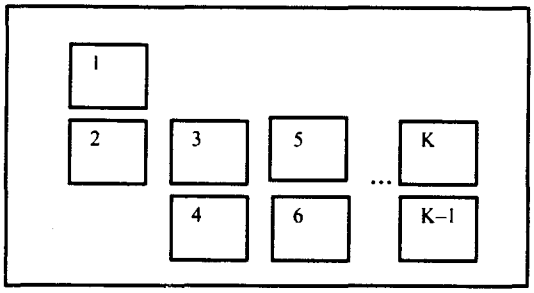

Figure 3 Layout of K digitized sub_images

A semi–automated system is used to register the K sub_images together with a human expert visually inspecting the sub_images and highlighting common features in neighboring images. A registration technique is then applied to compute the exact match between these features. Several registration techniques have been investigated [12]. In this work we have experimented the usage of two registration techniques (1) Coincident Bit Counting (CBC) registration method [13], and (2) Cross Correlation (CC) registration method [14] . Finally the overlapping areas of the registered sub_images were resolved.

D. Image Segmentation

The result of the registration phase is a large image of the complete LDM microcirculation, for clearer images and further analysis it is necessary to separate the blood vessels of interest from the background, and produce a binary image.

Several approaches exist for image segmentation, the first approach is image thresholding , in this technique all pixels with gray level above a certain threshold are classified as object, otherwise, they are classified as background. Thresholding limit can be set globally for the whole image, or locally computed in the neighborhood of each individual pixel.

Edge detection techniques can also be used to segment the images we are dealing with in this project [3]. A straight forward edge detection technique consists of applying a differential operator on the image. Differential operators give maximum response to edges, and minimum response to uniform background, however, they are highly susceptible to noise.

A more elaborate edge detection technique would utilize graph searching techniques for optimal edge detection [4]. First we apply a local operator to generate a set of candidate edge points, construct a graph with the edge candidates as nodes, and the costs of the links from one node to the other is set according to a formula depending on the relative positions of the two pixels, and the local operator's response at these two pixels, then search for the optimal edge using a graph searching technique. Algorithms published in [5], and [6] are two such methods.

Another class of segmentation algorithms region growing algorithms [7]. In these a seed pixel is found which is representative of the region. From this seed pixel the region is expanded with its neighboring pixels if those neighboring pixels meet a certain criterion based on their gray levels. The process is stopped when no more pixels can be added to the region. As Johnson discussed in his thesis, region growing techniques are very sensitive to the initial seed point, and are historically known to be slow [8].

Relaxation techniques [10],[11] were also attempted in our search for a proper segmenting algorithm. Relaxation is an iterative process which makes probabilistic classifications at every pixel at each iteration. The probabilities are adjusted at each iteration depending upon the presence of either supporting or conflicting evidence at neighboring pixels.

Bearing in mind the size of the image we have (2000x2000), and the necessity to detect most of the blood vessel network, we have abandoned the above mentioned techniques

due to their computational complexity and a simpler, more computationally efficient algorithm was sought.

The objective of this phase of our project was to develop a simple segmentation algorithm that requires minimum user intervention, and produces consistent results. The user defines the beginning and the end of a blood vessel segment, and the program iteratively determines the center–line, and the boundaries of the blood vessel between these two points.

The organization of this thesis is as follows, chapter II describes the methods used in the registration of the images, chapter III discusses the segmentation algorithm. Chapter IV presents the results of our work and a discussion of our results is presented in chapter V. Finally chapter VI contains conclusions and recommendations.

CHAPTER II
IMAGE RECONSTRUCTION

A. Image Registration

Image registration is the process of geometrically aligning two images of the same object. Several registration techniques exist in the literature [12]. The one implemented here is based on the CBC registration method [13].

The registration process takes a set S of K images, and outputs a displacement vector $v = [(x_2, y_2), ..., (x_k, y_k)]$, where (x_i, y_i) is the displacement between upper left corner of image i and the upper left corner of image 1.

To register two images, an NxN window, centered around point P_1 is selected from image I, and another point P_2 is selected from image II. These points are user selected in the current implementation.

The CBC function is defined as :

$$R(P_2) = \sum_{\Delta y=-N/2}^{\Delta y=N/2} \sum_{\Delta x=-N/2}^{\Delta x=N/2} F(I_1(P_1.x + \Delta x, P_1.y + \Delta y) \otimes I_2(P_2.x + \Delta x, P_2.y + \Delta y)) \qquad (1)$$

where $\otimes$ is the XNOR operator, and F(.) is a function that counts the number of bits set to 1 in its argument.

The peak of the CBC function determines the actual match point.

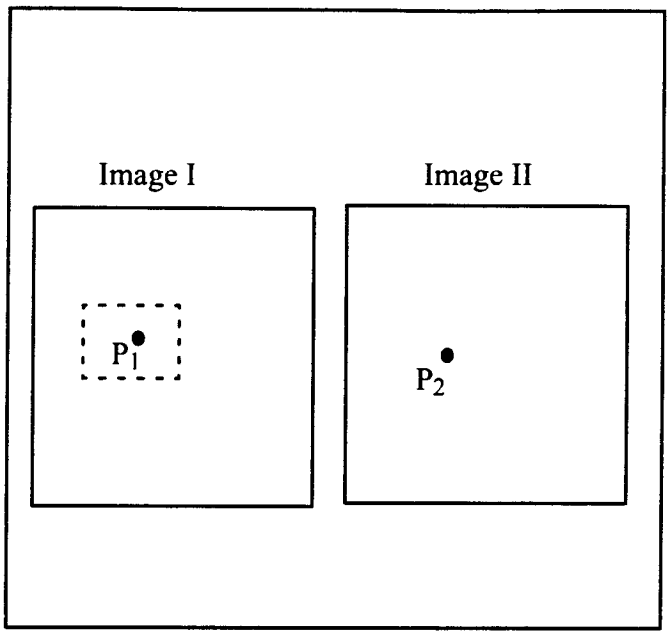

Figure 4 Input for Registration Method

The Cross–Correlation function is defined as :

$$R(P_2) = \sum_{i=0}^{i=N-1} \sum_{j=0}^{j=N-1} [I_1(P_1.x + \Delta x, P_1.y + \Delta y) - \mu_1] \cdot [I_2(P_2.x + \Delta x, P_2.y + \Delta y) - \mu_2] \quad (2)$$

Where

μ_1 is the average of window centered around P_1,

μ_2 is the average of window centered around P_2.

As in the CBC method, the peak of the registration surface indicates the best match. The means of which were subtracted to pronounce the registration surface peaks.

The illumination method used resulted in images with illumination maximum near the center of the image, and fades gradually as we move outwards. To compensate for that, the digitized sub_images were taken for highly overlapping areas. Captured sub_images were histogram equalized before registration.

B. Overlap Resolution

The result of the registration process is a set of overlapping images, an overlap resolution (OR) algorithm will resolve the grey level of pixels that overlap.

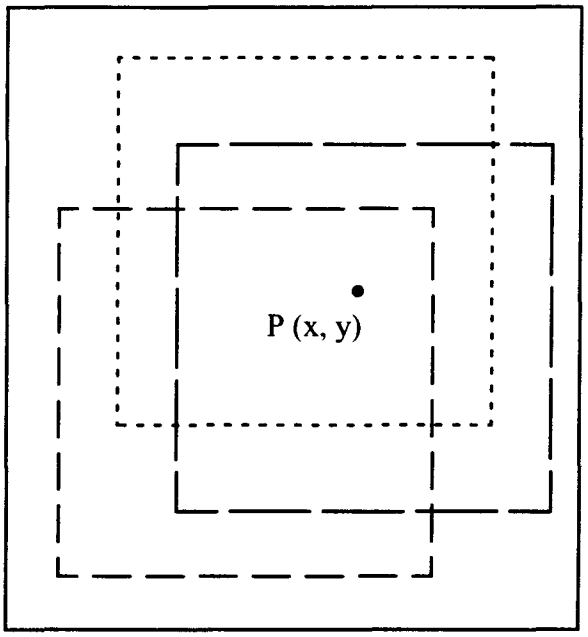

Figure 5 Outline of registered sub_images

In this work we have experimented with several filters for the overlap resolution, the Max filter was the only one which gave satisfactory results. Other filters we have experimented with were Average Filter, Average Filter with Clipping, Max Contrast Filter, and Max contrast Filter with Clipping.

1. Max Filter

Let O be the set of images overlapping at point P(x,y), Figure 5 , the grey level assigned to P is

$$I(x,y) = \max_{i \in O}(I_i(x,y)) \qquad (3)$$

2. Average Filter

In this filter the grey level of the overlapping pixels is resolved by taking their average.

3. Average Filter with Clipping

This has the same idea as the above filter, pixels with grey levels above a certain threshold, or below another threshold were discarded from the averaging process.

4. Max Contrast Filter

In this filter, the contrast of an MxM window centered around each pixel is computed, we resolve the grey level of the overlapping pixels by selecting the grey level of the pixel with highest window contrast.

5. Max Contrast Filter with Clipping

Same as Max Contrast filter, pixels with window contrast values above or below certain threshold were discarded.

Filters (2)–(5) above resulted in images with step change in illumination across sub_image boundaries (Figure 7), and in loss of information in parts of the resultant image (Figure 6). The Max filter was able to overcome these problems and resulted in uniformly illuminated constructed image while preserving all the details of the original sub_images.

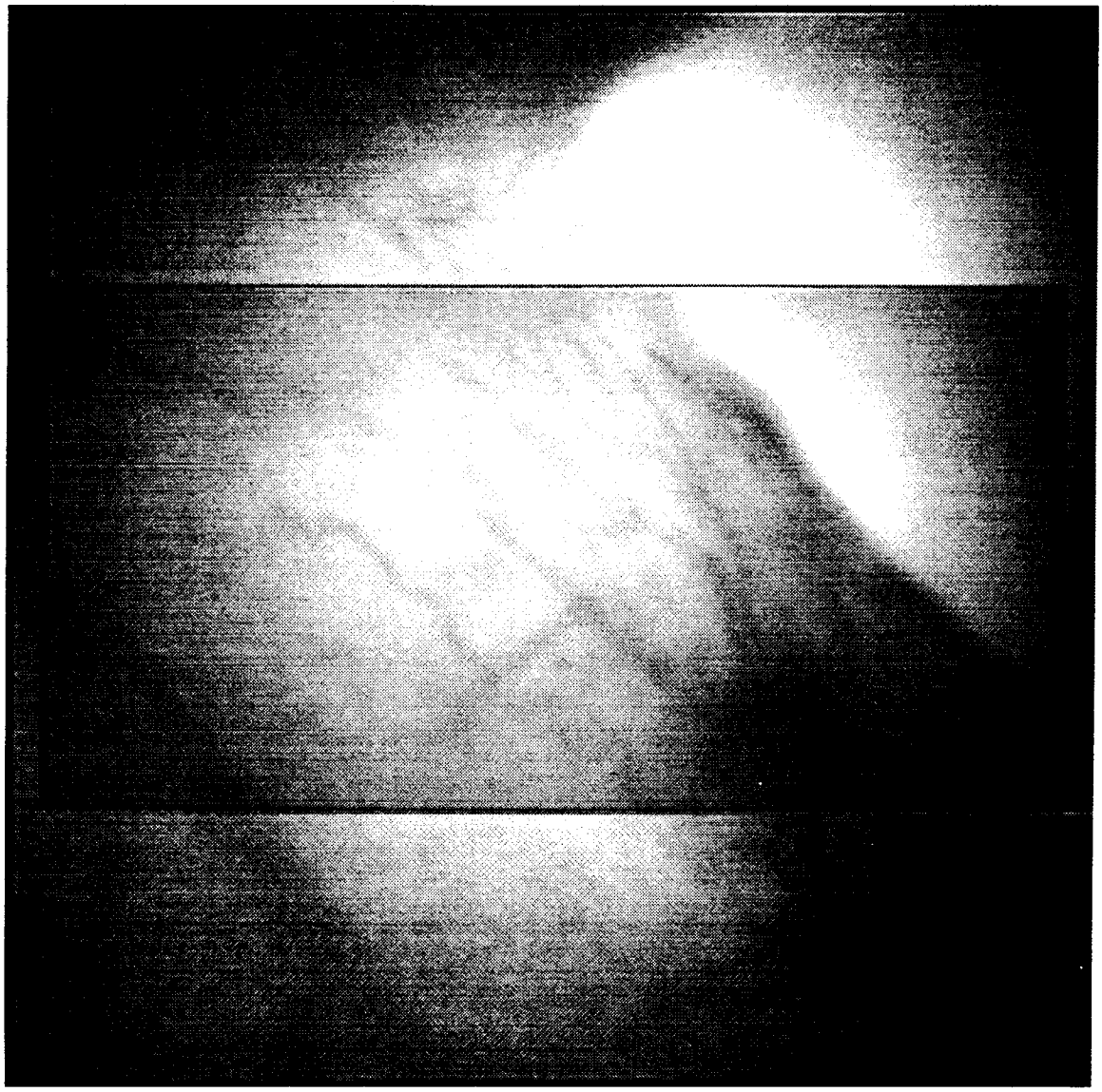

Figure 7 Overlap resolution by Average Filter

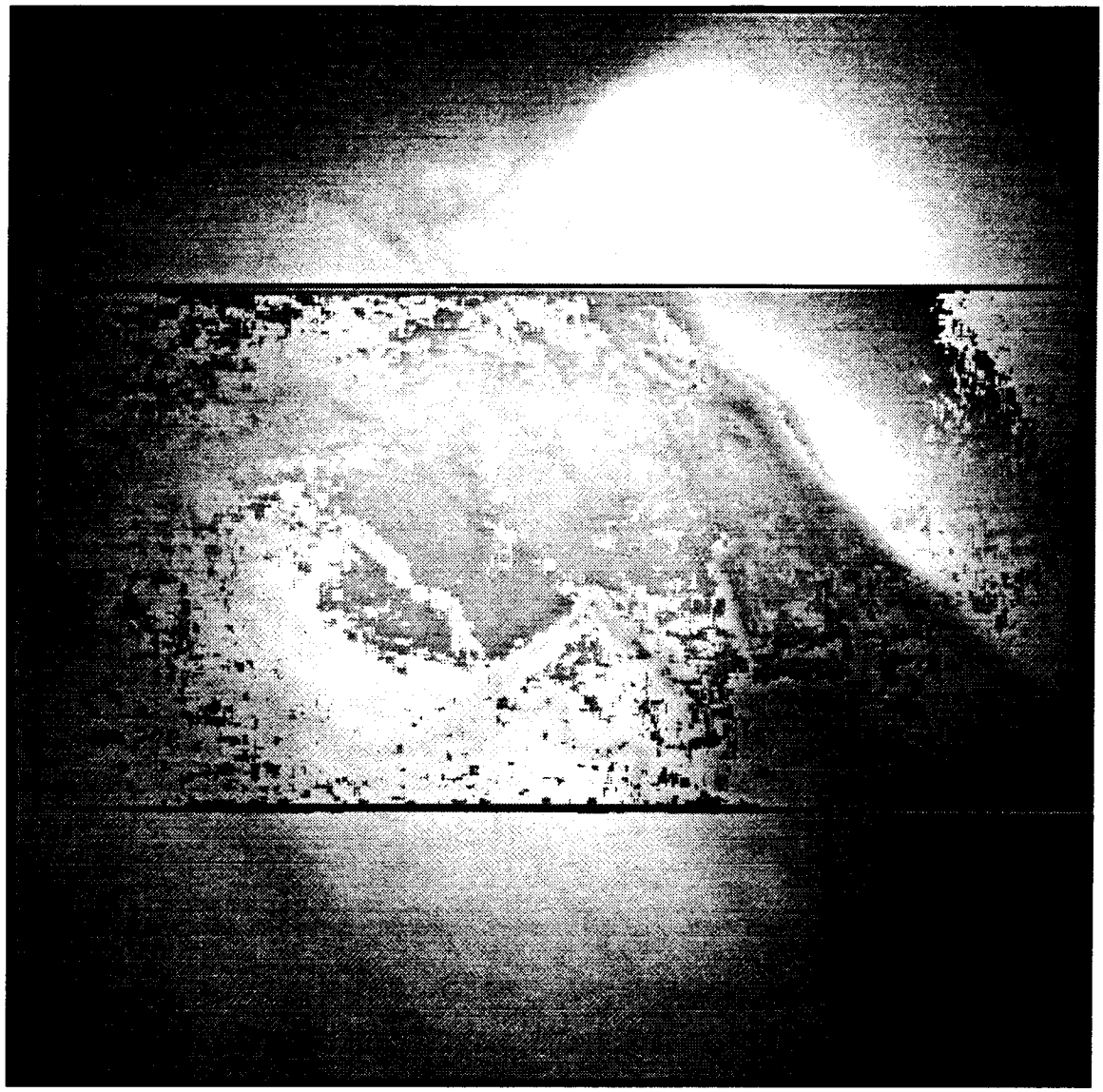

Figure 8 Overlap resolution with Max Contrast Filter

C. Reconstruction Procedure

Due to hardware constraints, the developed system displays up to six sub_images at a time. Therefore the captured sub_images have to be registered and merged in two steps. First step produces intermediate images from the captured sub_images. Second step the intermediate images are registered and merged together to form the final image.

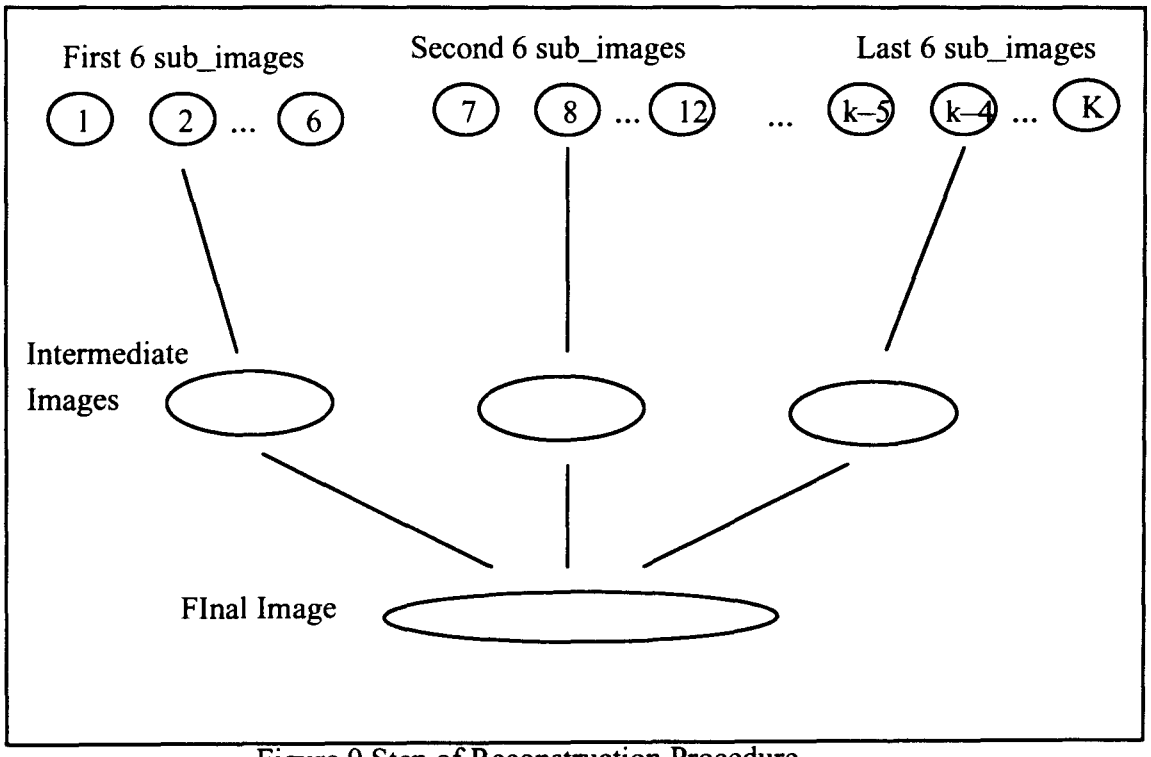

Figure 9 Step of Reconstruction Procedure

CHAPTER III
IMAGE SEGMENTATION

In our implemented algorithm, a human expert visually examines the image, and defines two points, (A, and B), each at one end of a section of a vessel segment with small curvature. Figure 10 (a) illustrates an example of this selection.

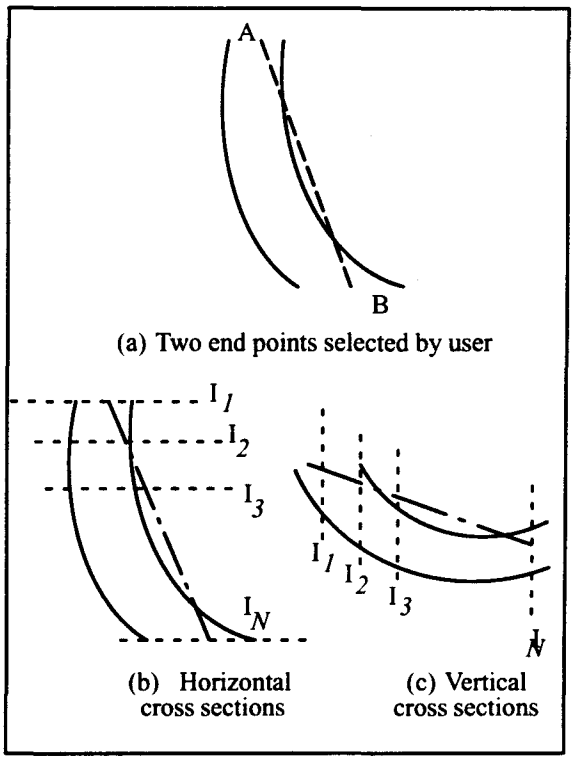

Figure 10 Cross sections defined by edge detection algorithm.

N equispaced cross sections of the vessel segment under study are then obtained. These cross sections are all parallel, and are either vertical or horizontal as determined by the following rule, if $|\Delta x| < |\Delta y|$, then cross sections are horizontal, else they are vertical. In the above rule $\Delta x = x_A - x_B$, and $\Delta y = y_A - y_B$, Figure 10 (b)–(c) illustrate these two cases. These cross sections will produce N intensity profiles I_i, $i = 1 .. N$, Figure 11 shows the gray

level distribution across one profile. The width of each cross section is constant and equal to W, these N cross sections are centered around the line segment AB.

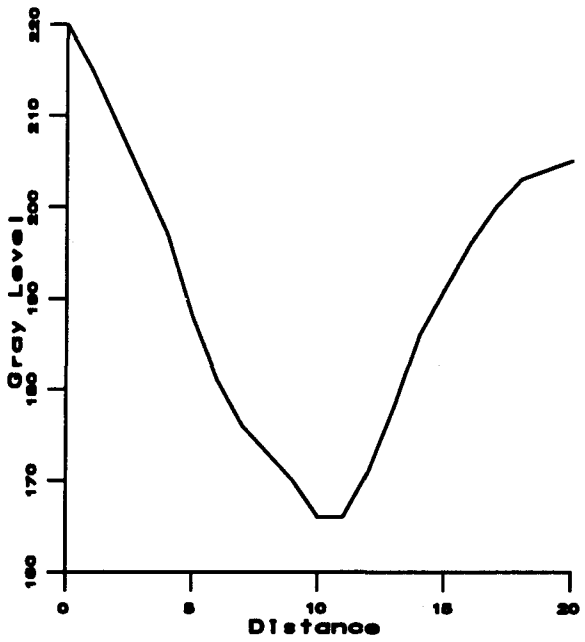

Figure 11 Intensity profile at a cross section

The following 4 procedures are then applied on each cross section.

A. Center Point Detection

Examine profile I_i, and find the point with minimum gray level P_i. P_i will be taken as the initial estimate of the midpoint of the blood vessel at cross section *i*.

B. Edge Detection

For each profile I_i, find the two points d_{i1}, and d_{i2}, defined by the following equation:

$$I_i(d_{i1}) = KC_{i1} + I_i(P_i) \qquad (4)$$

$$I_i(d_{i2}) = KC_{i2} + I_i(P_i) \qquad (5)$$

where , C_{i1} is the contrast at cross section i to the left of P_i, C_{i2} is the contrast at cross section i to the right of P_i, and K is an empirical constant.

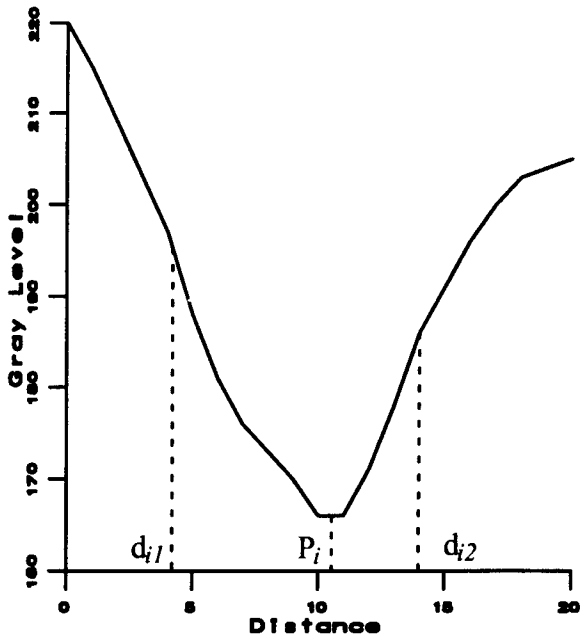

Figure 12 Edge interpolation at a cross section

C. Center Point Interpolation

The center point of the segment at cross section i is taken is the midpoint between the two edge points detected in the previous step.

D. Filling Algorithm

Filling of the vessel body is achieved by filling in the spaces between the cross sections. For each space in between two cross sections, we draw a set of lines having the same orientation as that of the cross sections. Each line will have one end point on the line segment d_{i1} $d_{(i-1)1}$, and the other end point on d_{i2} $d_{(i-1)2}$.

E. Cascaded Sections of a Vessel Segment

For long vessel segments with high tortuosity, we have added an internal mechanism to ensure the continuity of center line detected, as well as the smoothness of the edges.

The user will click on several points along the vessel segment, such that the section enclosed between any two consecutive points is of low curvature. For each section , the algorithm is applied to detect the center line and edges. From one section to the next, a straight line is drawn to connect the end point of the center line of the first section with the start point of the center line of the second section. To ensure edge continuity from one section to the other within one vessel segment, a straight line is draw to connect edges of one section to those of the next.

F. Segments with Bifurcations

Figure 13 represents a sample of two intersecting vessels. The algorithm should be applied to vessel 1 first. When applying the algorithm to vessel 2, the algorithm extends the center line of vessel 2 until it intersects with the center line of vessel 1. The edges of vessel 2 are drawn until they intersect with the edges of vessel 1. In the current implementation, the user must select P_1 (first point on vessel 2) such that it falls on the body of vessel 1.

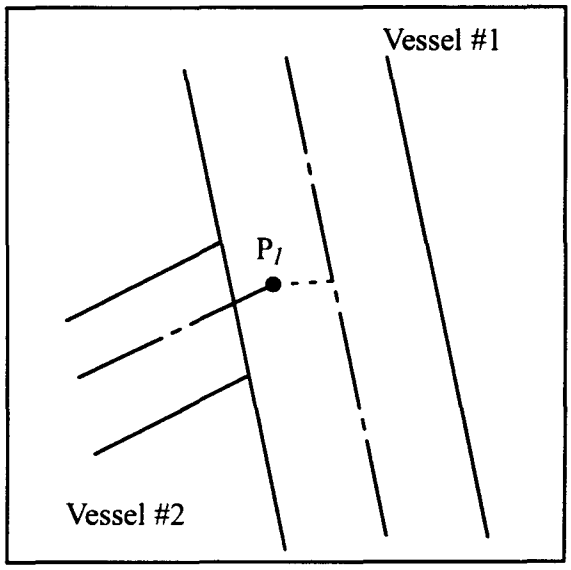

Figure 13 Segmenting Bifurcated Vessels

G. Image Preprocessing

The images were scaled down to 50% of their original size, and a smoothing 3x3 filter was applied to the whole image. The scaling allowed us to manipulate the images within our limited disk resources while preserving all the vessels' qualities.

H. Quantification

The following measurements were done on the vessel segments being segmented. Data was collected while the algorithm was running. The length L of the vessel is the length of its center line, the area A of the vessel is the number of pixels drawn between the edges of the vessel, the straight line length S is the direct distance between the start of the center line of a vessel segment and the end point.

Based on the above definition of L, S, and A, we can define the following equations

1. Diameter (D)

$$di = \frac{A_i}{L_i} \qquad (6)$$

$$d = \frac{\sum_{i=0}^{M-1} L_i d_i}{\sum_{i=0}^{M-1} L_i} \qquad (7)$$

Where d_i is the diameter of vessel segment i, and d is the weighted average diameter for M vessel segments.

2. Tortuousity (T)

$$T_i = \frac{L_i - S_i}{S_i} \qquad (8)$$

$$T = \frac{\sum_{0}^{M-1} L_i * T_i}{\sum_{0}^{M-1} L_i} \qquad (9)$$

Where T_i is the toruousity of one vessel segment i, T is the tortuousity of M vessel segments.

I. Other Attempted Algorithms

We attempted several algorithms before instituting the one actually implemented. Relaxation techniques and dynamic thresholding were experimented with and both failed to give satisfactory results.

In dynamic thresholding technique, we followed the method Rapson [15] implemented for calculating the optimum gray level threshold, experimenting with several region sizes. All attempts failed to give satisfactory results. Often the background tissues were misclassified as blood vessels, and some vessels with low contrast were misclassified as background.. Figure 14 shows the result of running the dynamic thresholding algorithm on a complete LDM.

We also experimented with relaxation techniques. This technique proved to be inappropriate for several reasons, first the computational complexity was very high, and second the results were not as expected. Figure 15 shows the results of running the relaxation algorithm on a complete LDM.

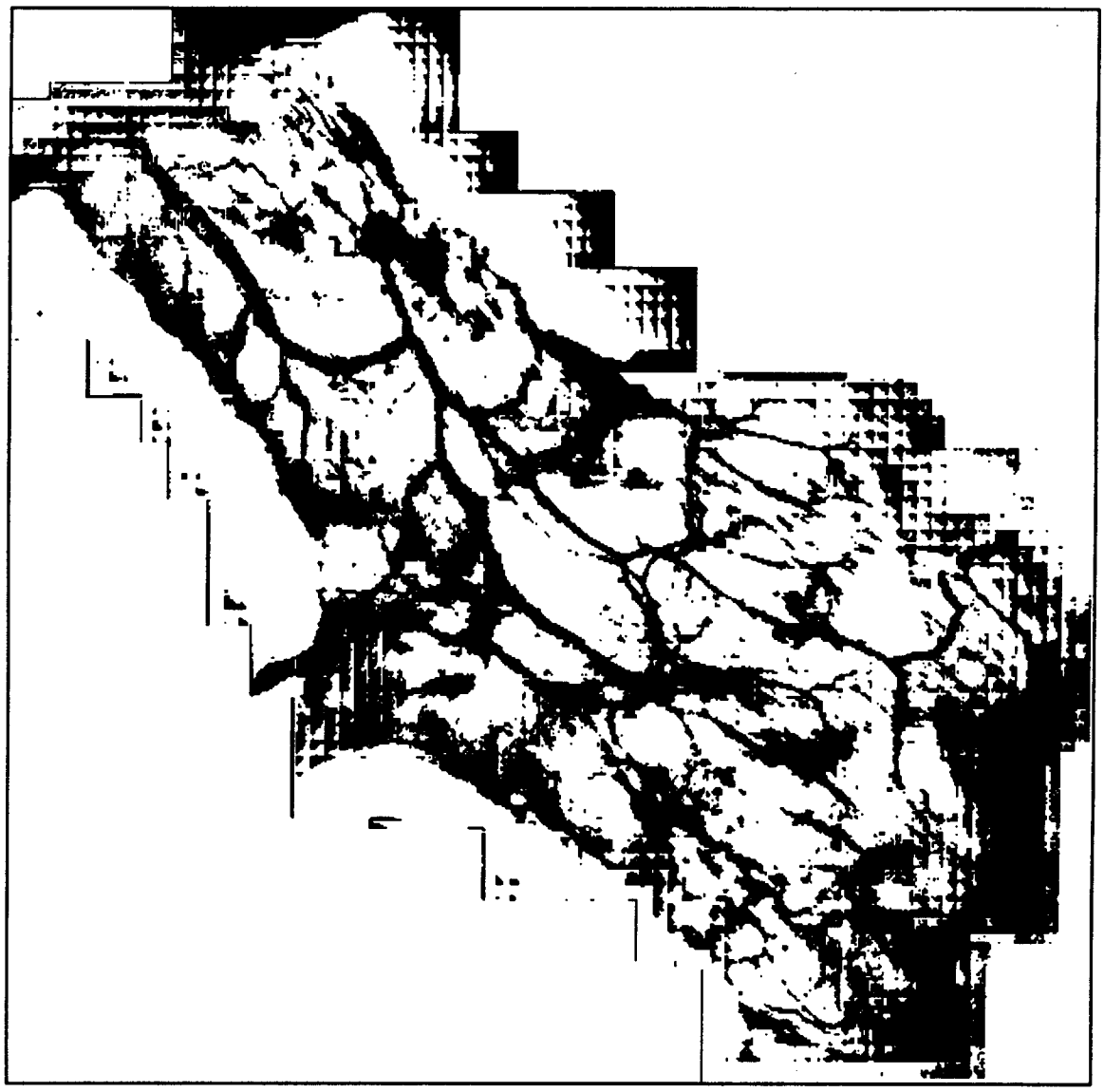

Figure 14 Output of Dynamic Thresholding Algorithm

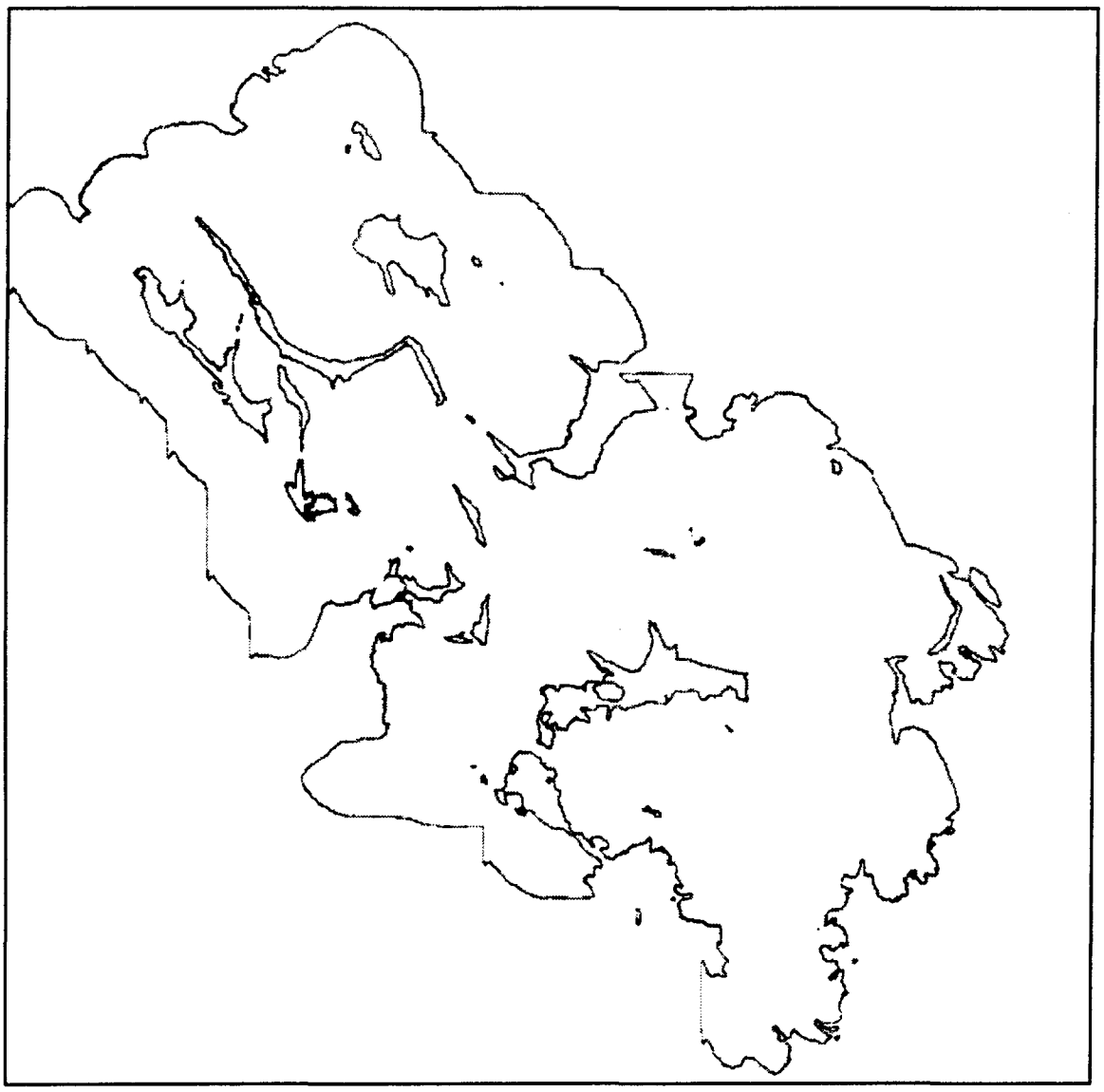

Figure 15 Output of Relaxation Method

CHAPTER IV
RESULTS

A. Image Registration

In this section, the CBC registration method is evaluated and compared to the Cross Correlation (CC) registration method [14], the results of registering six digitized sub_images and the resultant image is presented. The result of reconstructing a complete LDM is also presented.

1. Results of CBC Method

A sample digitized sub_image of 640x480 resolution was used (Figure 16). A window of size 30x30 centered at point P_1 was selected surrounding a major feature in the image. The CBC method was then used to determine the correct position of the window in the sub_image. The search was performed in a neighborhood of 30x30 surrounding an initial point P_2.

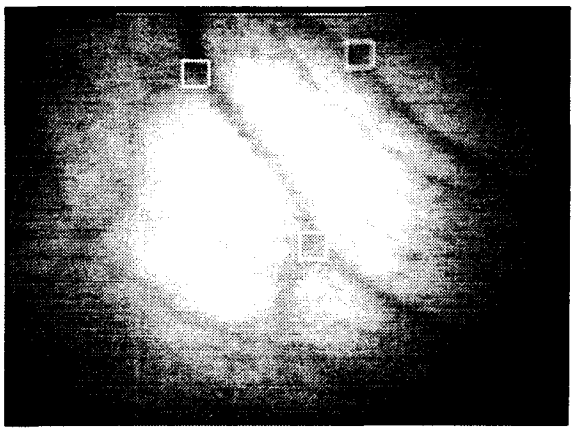

Figure 16 A Sample digitized sub_image

	Test Case I		Test Case II		Test Case III		Test Case IV	
P1	P_2	(Δx,Δy)	P_2	(Δx,Δy)	P_2	(Δx,Δy)	P_2	(Δx,Δy)
(216,75)	(216,75)	(0,0)	(216,80)	(0,–5)	(221,75)	(–5,0)	(221,80)	(–5,–5)
(350,271)	(350,271)	(0,0)	(350,276)	(0,–5)	(355,271)	(–5,0)	(355,276)	(–5,–5)
(402,53)	(402,53)	(0,0)	(402,58)	(0,–5)	(407.,53)	(–5,0)	(407,58)	(–5,–5)

Table 1 Summary of CBC Test Cases.

The method was tested for three different windows (outlined in Figure 16). For each window, four different values for P_2 were tested. For each test case the surface of the registration method was plotted, and the displacement (Δx,Δy) between the peak of the surface and P_2 was calculated. Table 1 summarizes the 12 test cases. Table 2 shows the running times for the CBC registration method as well as the Cross–Correlation method. Figures 5–7 are samples of the registration surfaces' plots. The CBC method was able to determine the correct position for all the test cases.

	CBC	Cross–Correlation
Minimum	1.06	0.72
Maximum	1.20	0.75
Average	1.144	0.738

Table 2 Running Times for the Registration Methods.

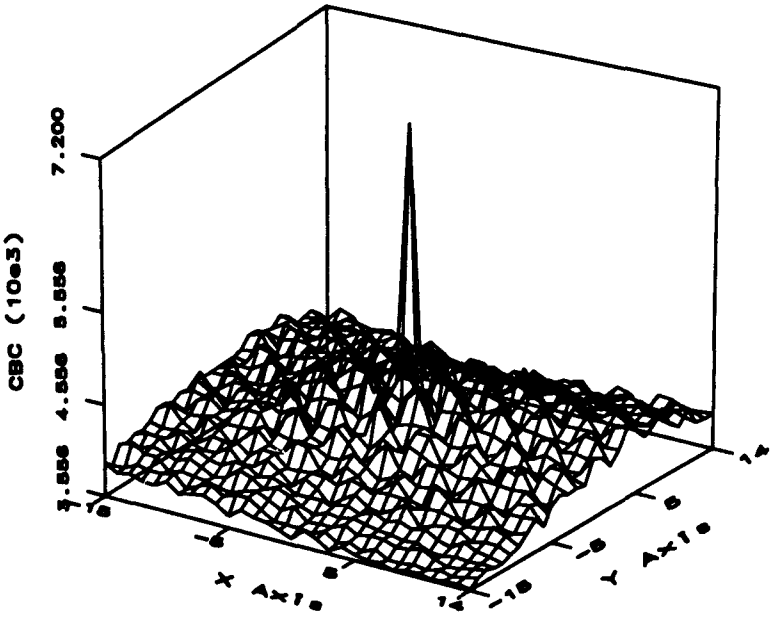

Figure 17 CBC Registration Surface : P1 (216,75) P2 (216,75)

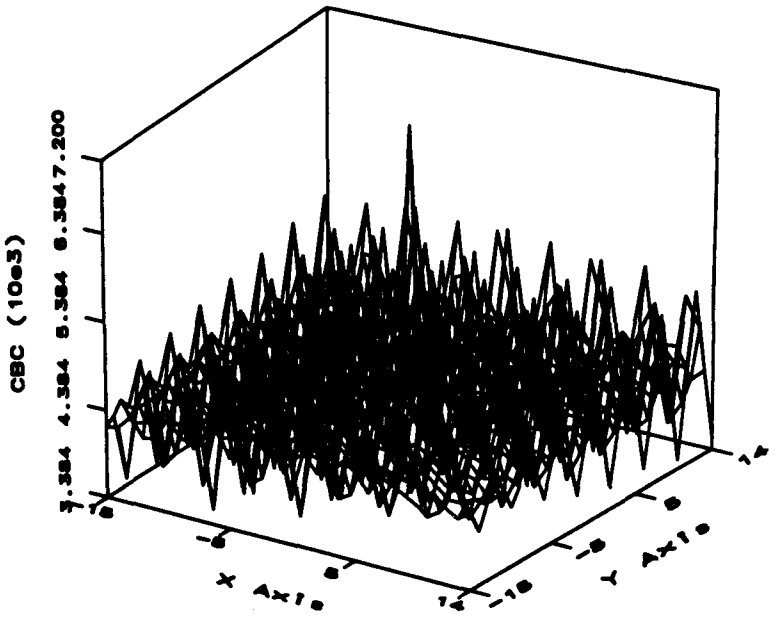

Figure 18 CBC Registration Surface: P1 (350, 271) P2(350, 271)

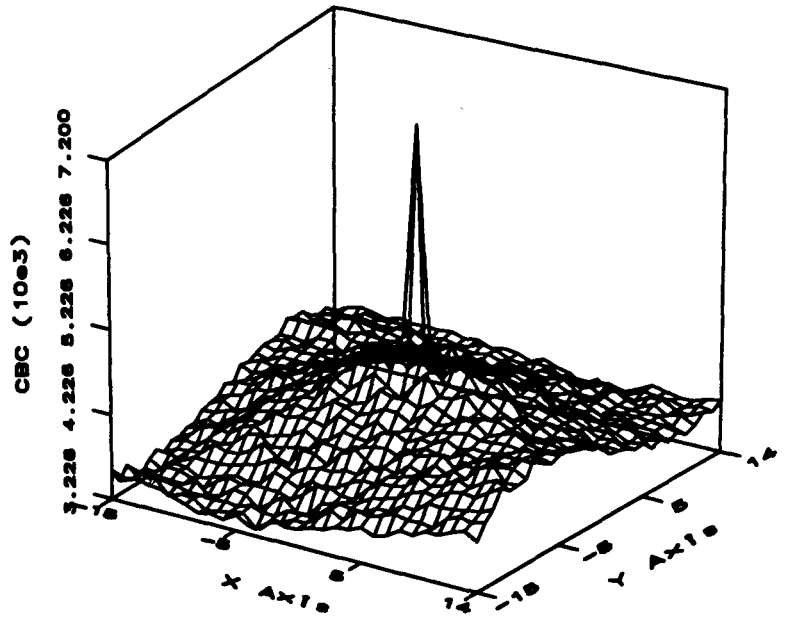

Figure 19 CBC Registration Surface: P1 (402,53) P2 (402,53)

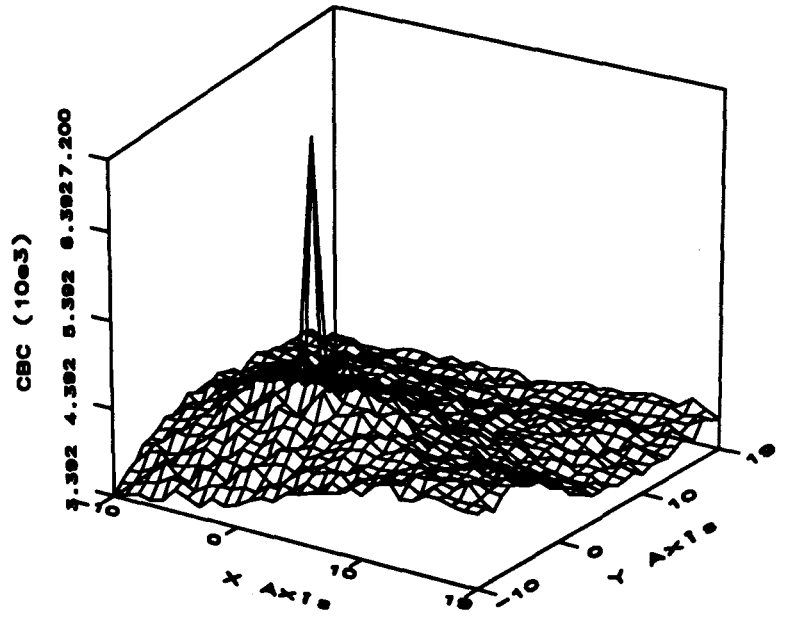

Figure 20 CBC Registration Surface: P1 (402,53) P2 (407,58)

2. Results of the Cross–Correlation method

The results of Cross–Correlation registration method are presented here. The test cases used here are the same as that used in evaluating the CBC method. This method was able to determine the correct match for all the test cases described earlier, however the peaks are not as clear as those resulting form the CBC method. Figures 9–11 are samples of the registration surfaces' plots.

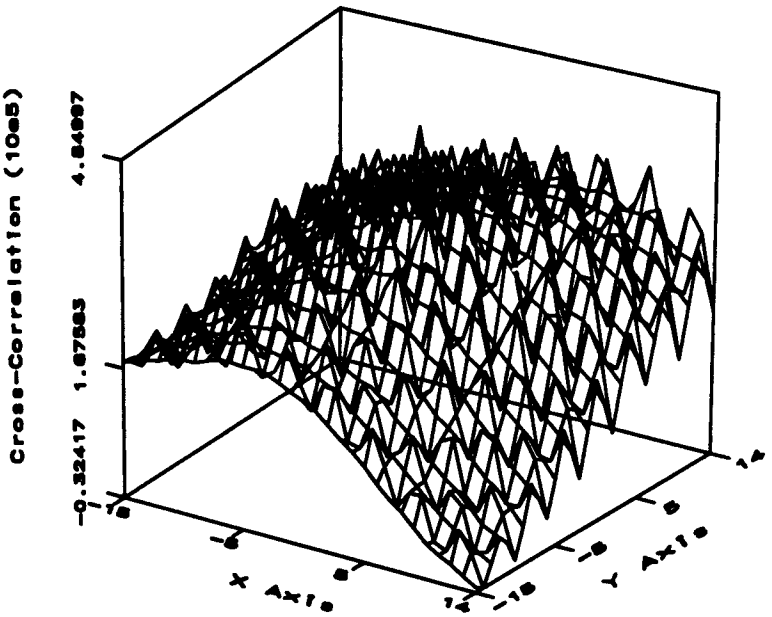

Figure 21 CC Registration Surface: P1 (216, 75) P2 (216,75)

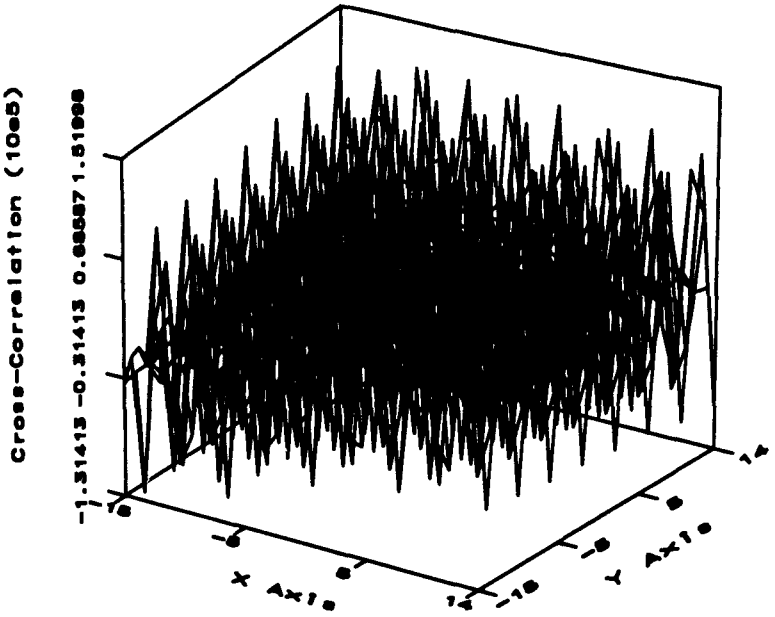

Figure 22 CC Registration Surface: P1 (350,271) P2 (350,271)

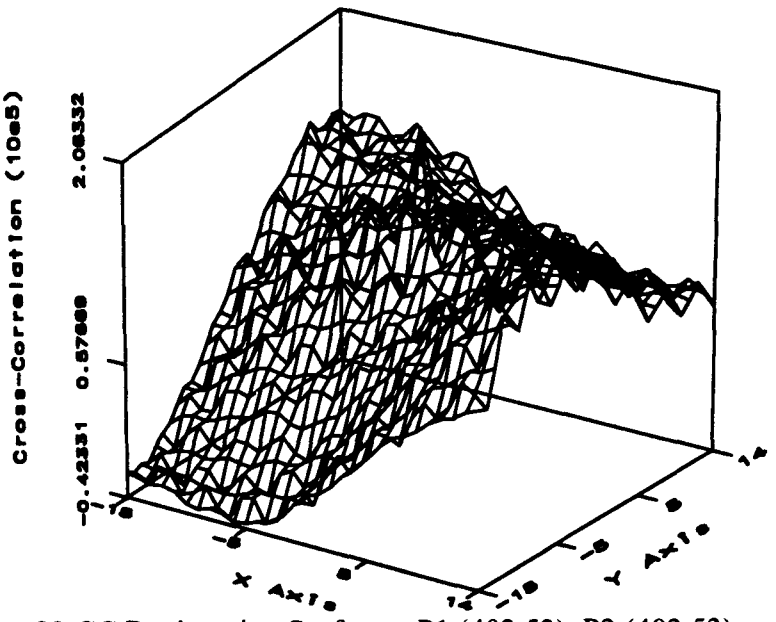

Figure 23 CC Registration Surface: P1 (402,53) P2 (402,53)

B. Image Reconstruction

Figure 24 shows a sample of the digitized sub_images, each is of resolution 640x480x256. The result of the registration process is shown in Figure 25 . Figure 26 shows the outline of the registered sub_images. Figure 27 is the result of applying the overlap resolution algorithm. The total number of sub_images digitized for this sample was fifty five. Six sub_images were registered at a time, resulting in nine intermediate images. The same technique was repeated several times until the complete LDM image was reconstructed (Figure 28)

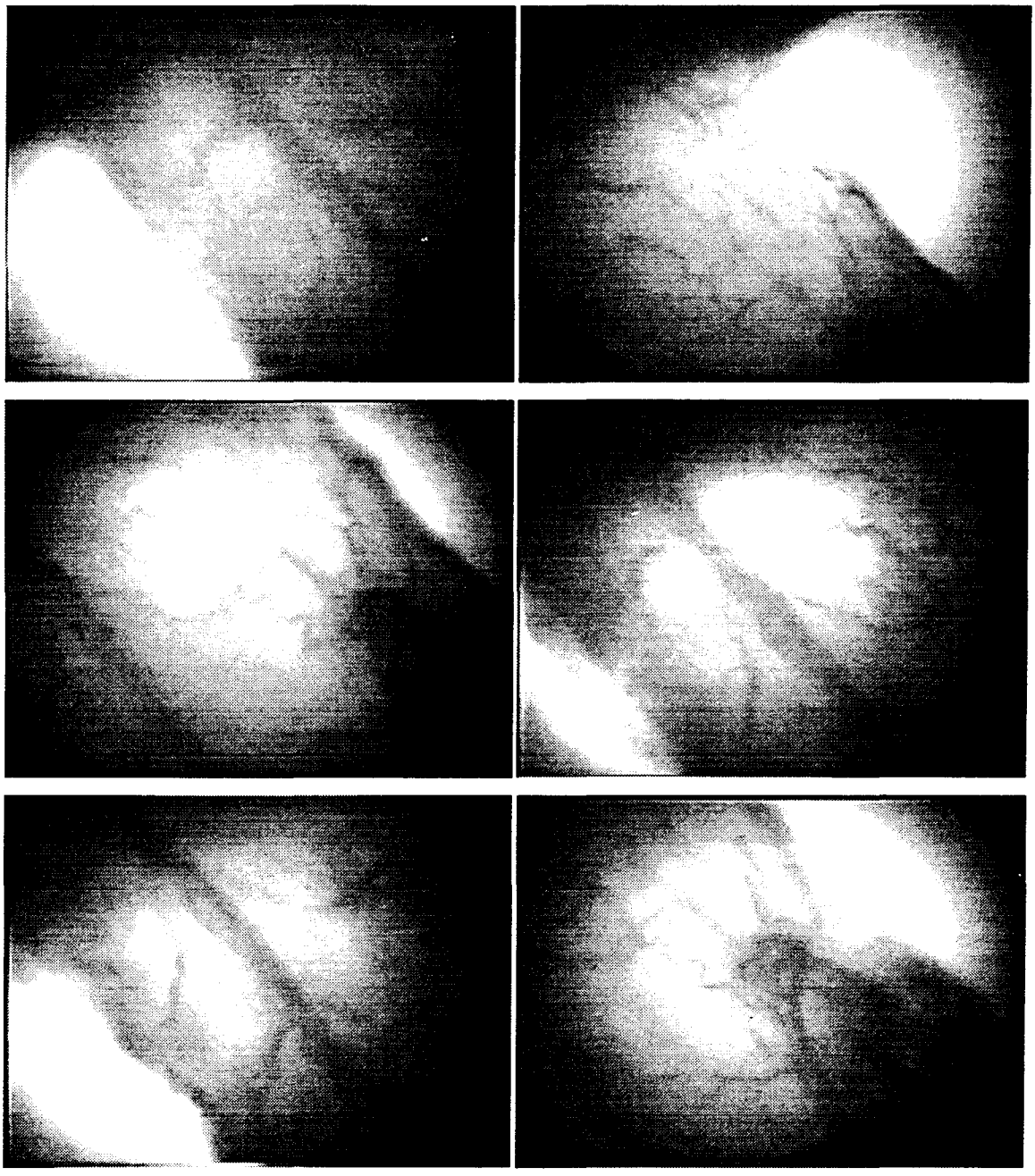

Figure 24 Sub_images used in the registration process

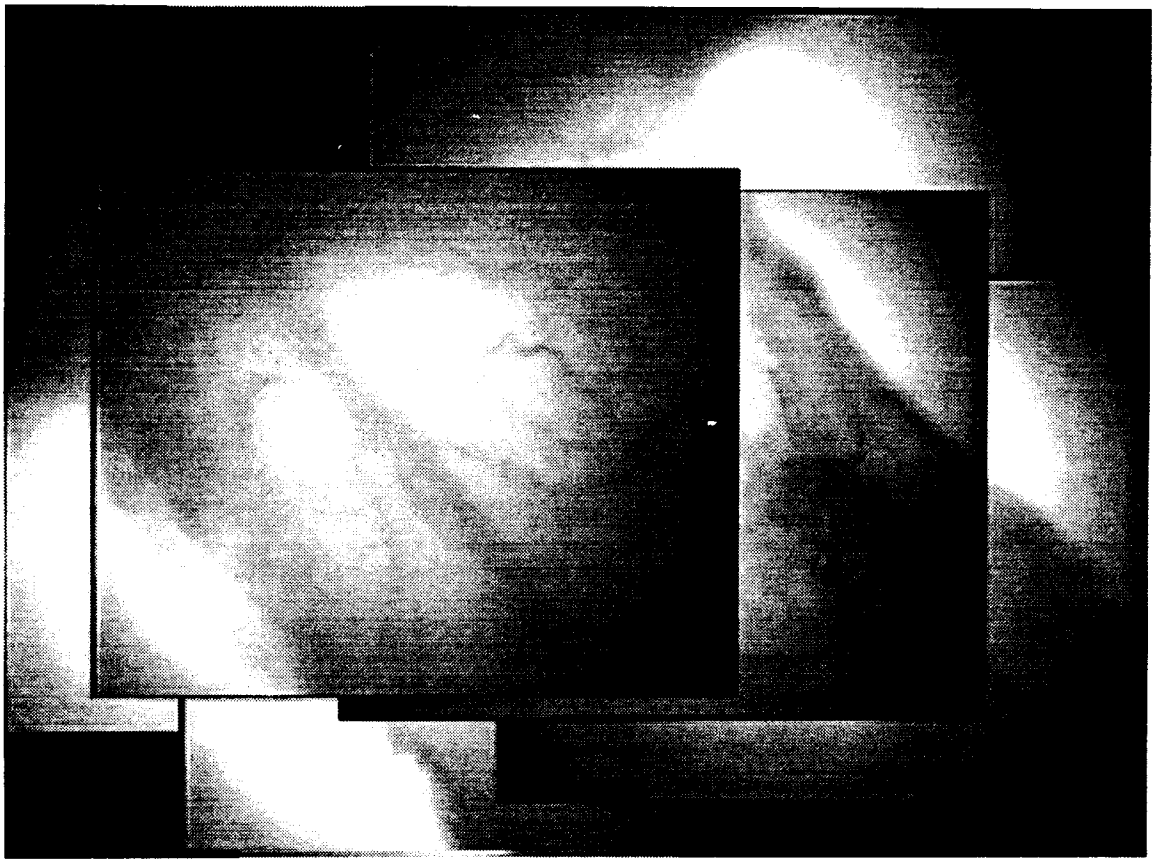

Figure 25 Result of Registration Process

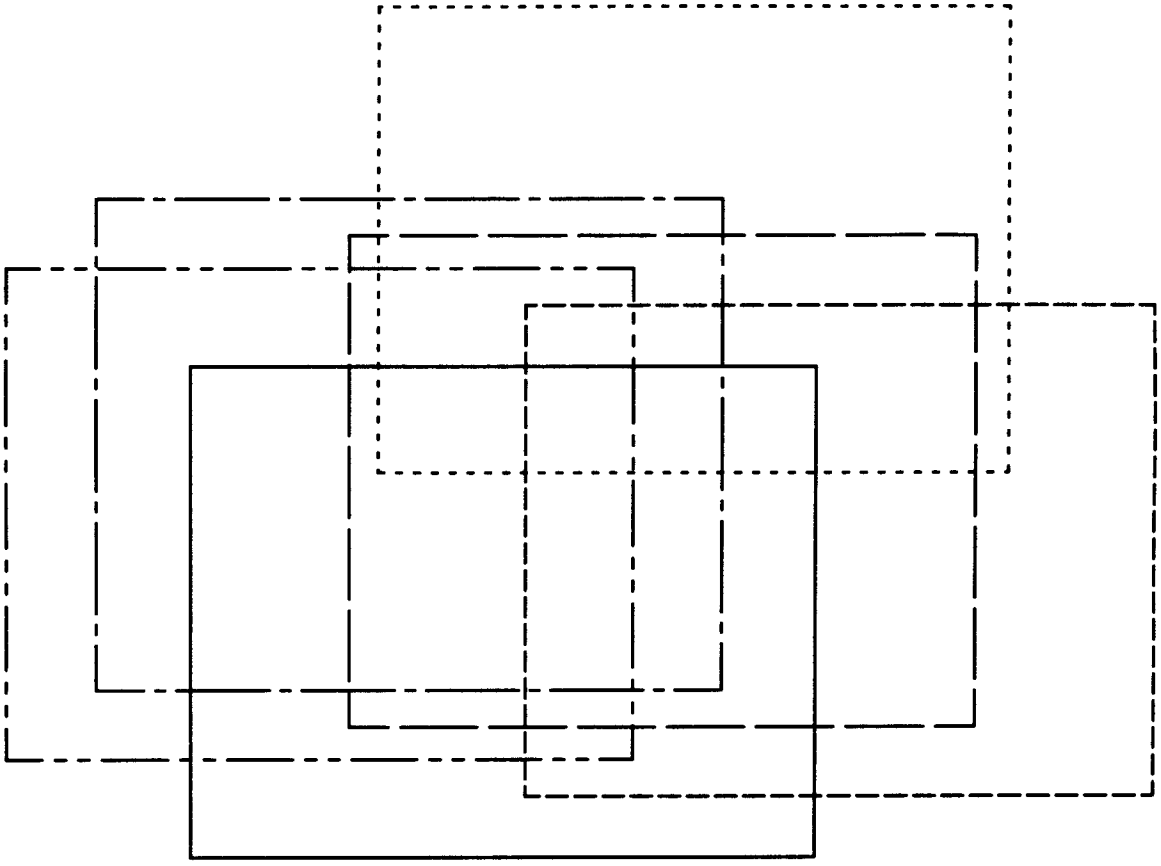

Figure 26 Outline of the registered sub_images

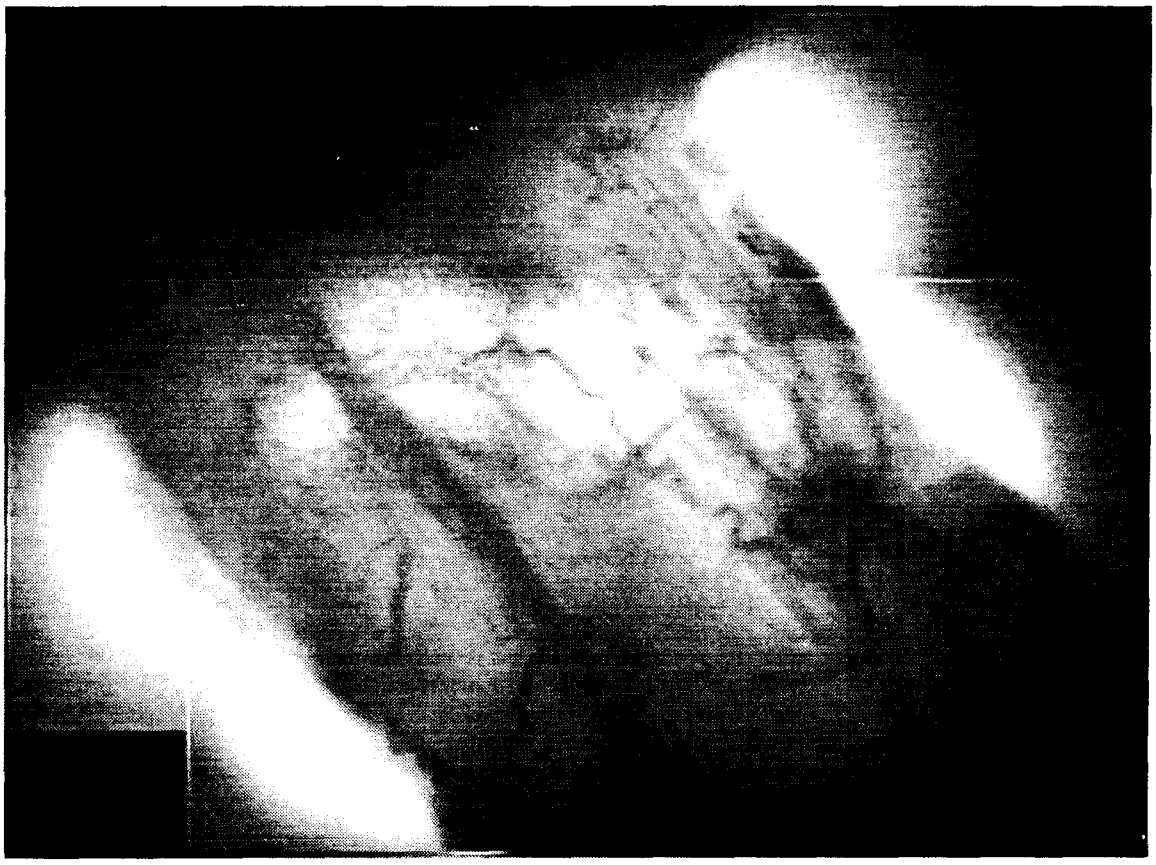

Figure 27 Overlap resolution

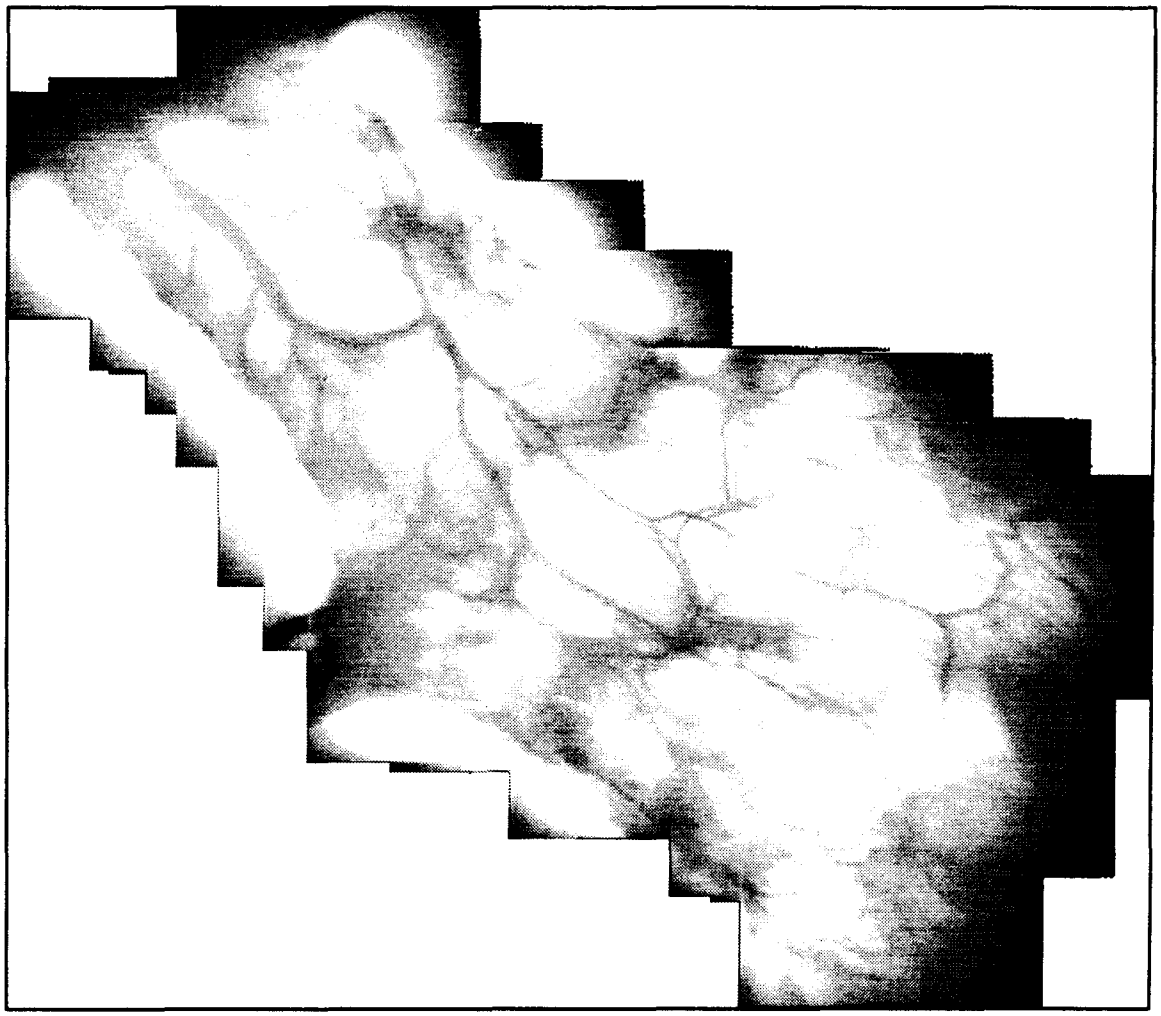

Figure 28 Completed LDM muscle image (Black background removed)

C. Image Segmentation

The value of W was 30, and N was chosen such that the separation between the cross sections was 4 pixels. The first and last cross section must intersect with points A, and B respectively.

Figure 29 is a vessel segment, with a low curvature. Figure 30 shows the gray level distribution in the neighborhood of this segment. Figure 31 – Figure 33 show the resulting center line, edges and vessel body as detected by our algorithm.

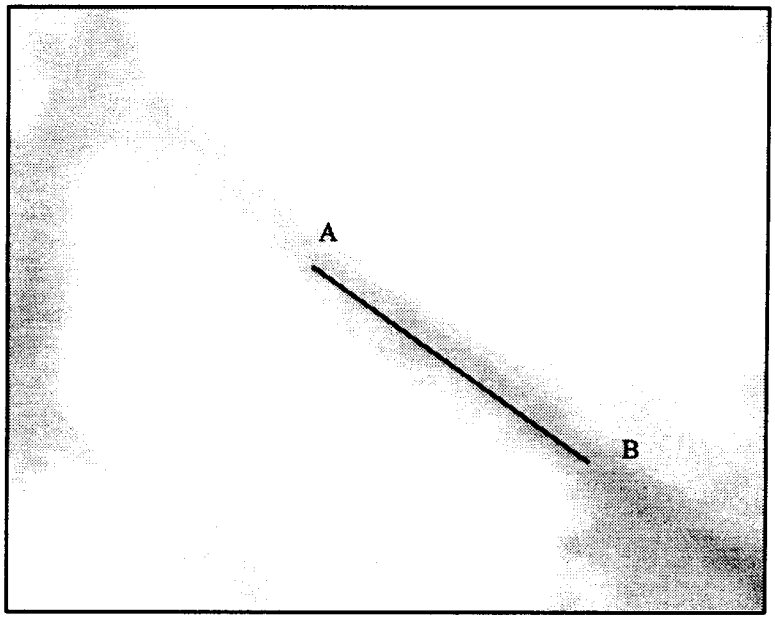

Figure 29 A sample vessel segment

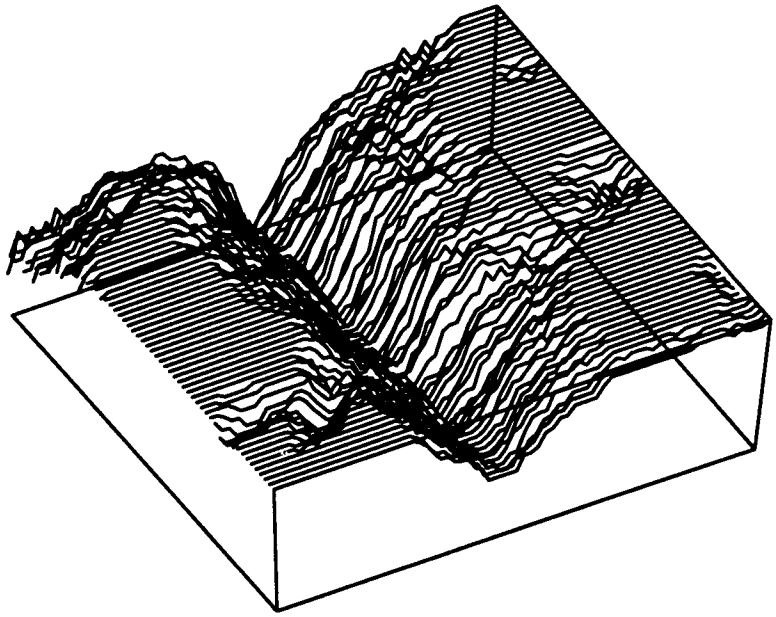

Figure 30 Gray level distribution

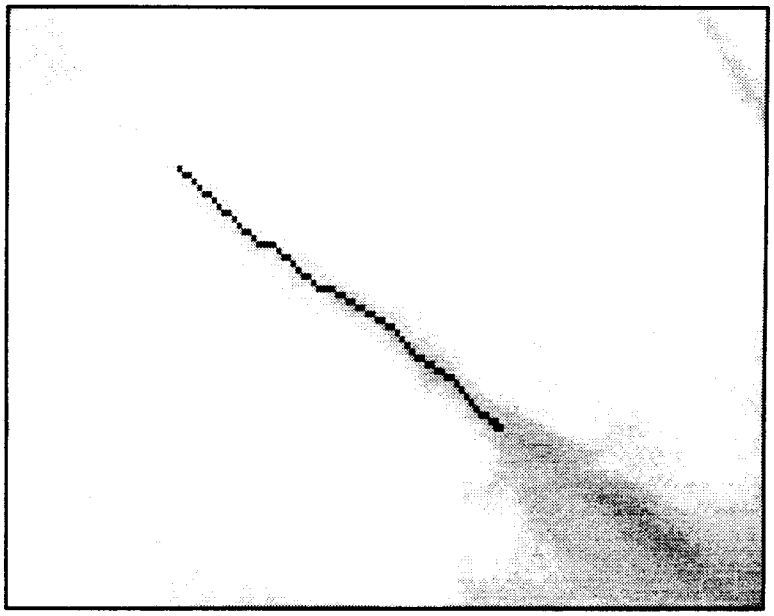

Figure 31 Center line

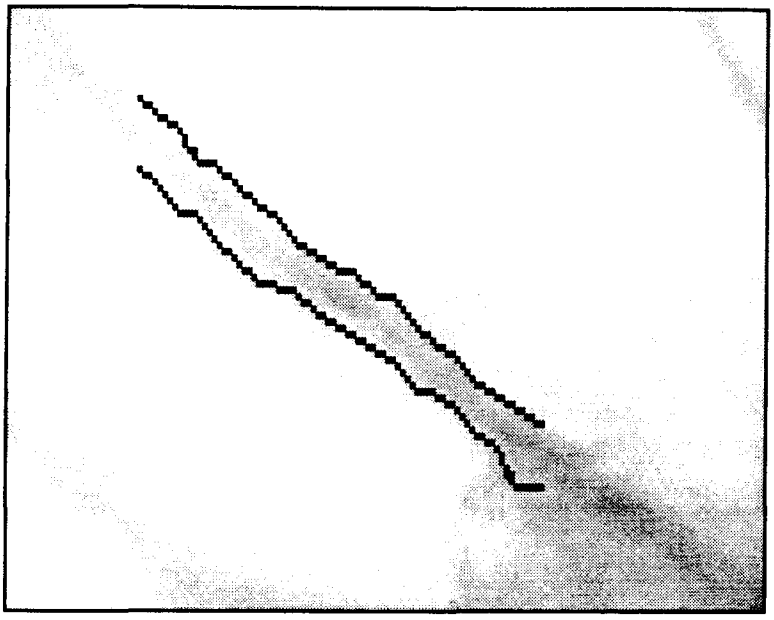

Figure 32 Edges

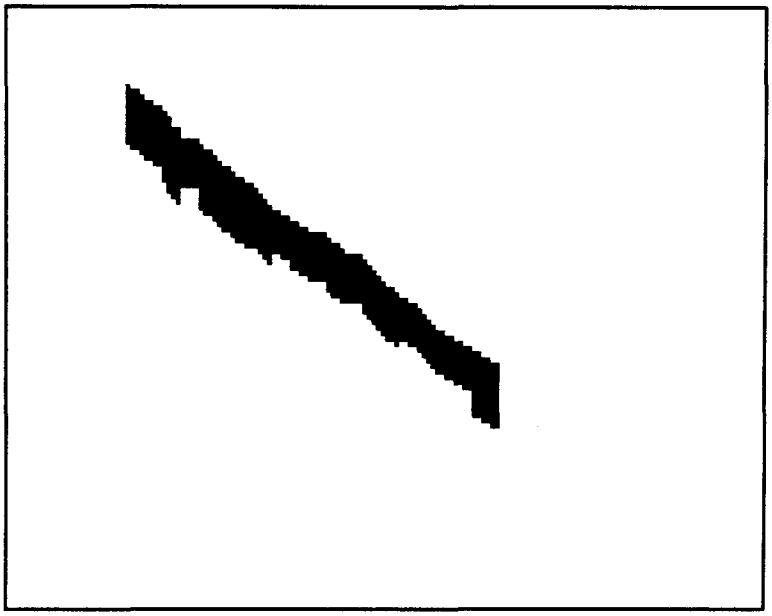

Figure 33 Vessel body

Figure 34 shows the results of running our proposed algorithm on a complete LDM. The values of W, and N are the same as in the previous example. The total time required by the user to determine the end points for each vessel segment was 20 minutes. Figure 35 shows the output edges, and finally Figure 36 is the segmented vessel body.

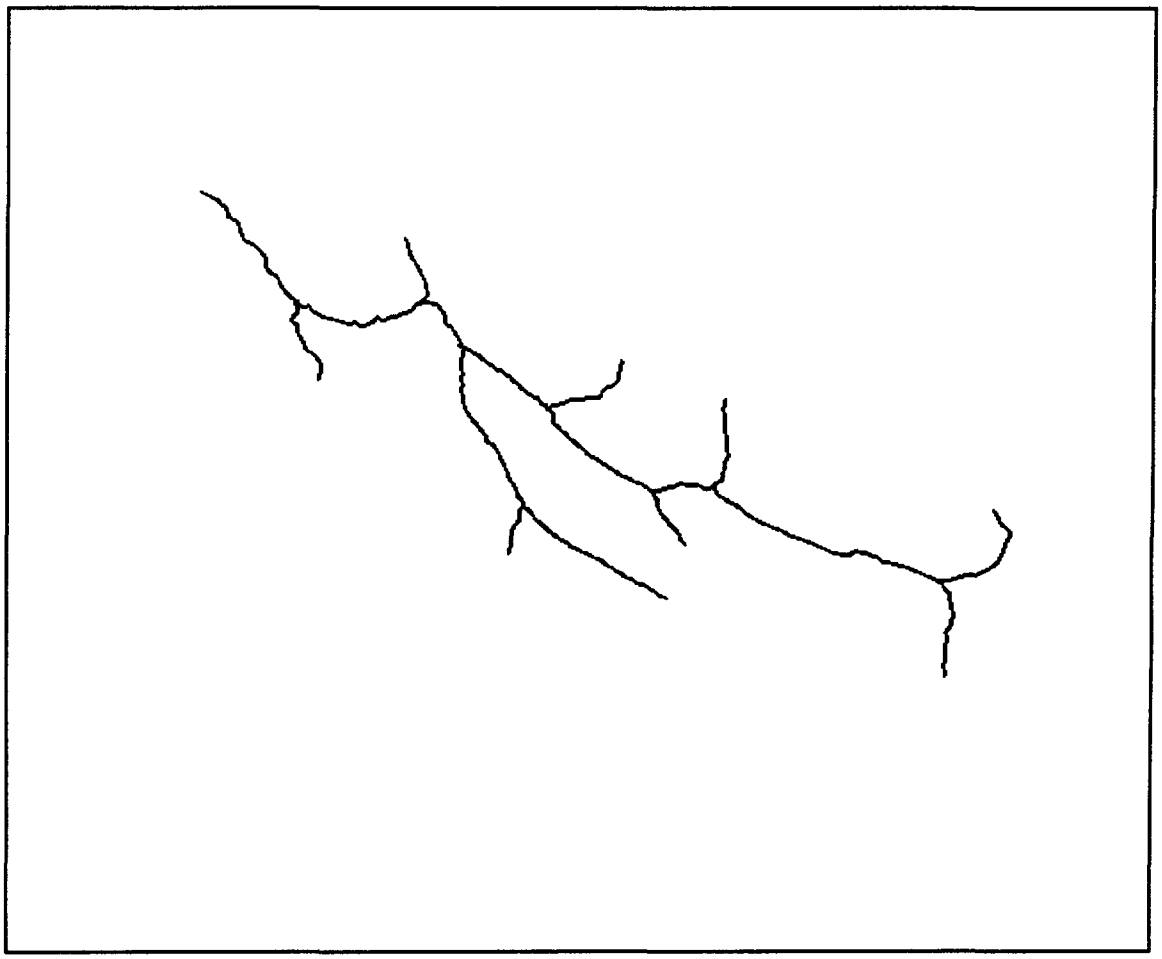

Figure 34 Center line of a complete LDM muscle

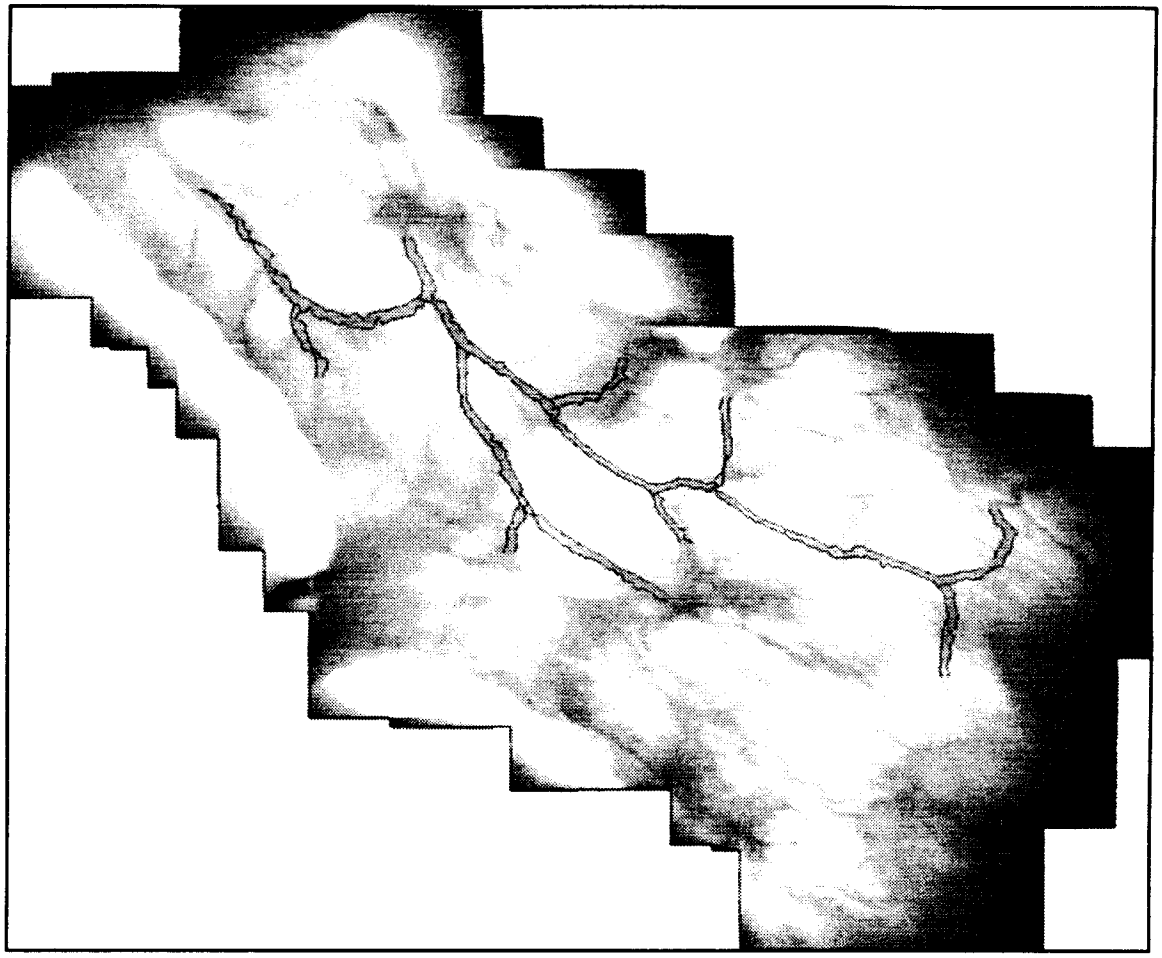

Figure 35 Edges of a complete LDM muscle

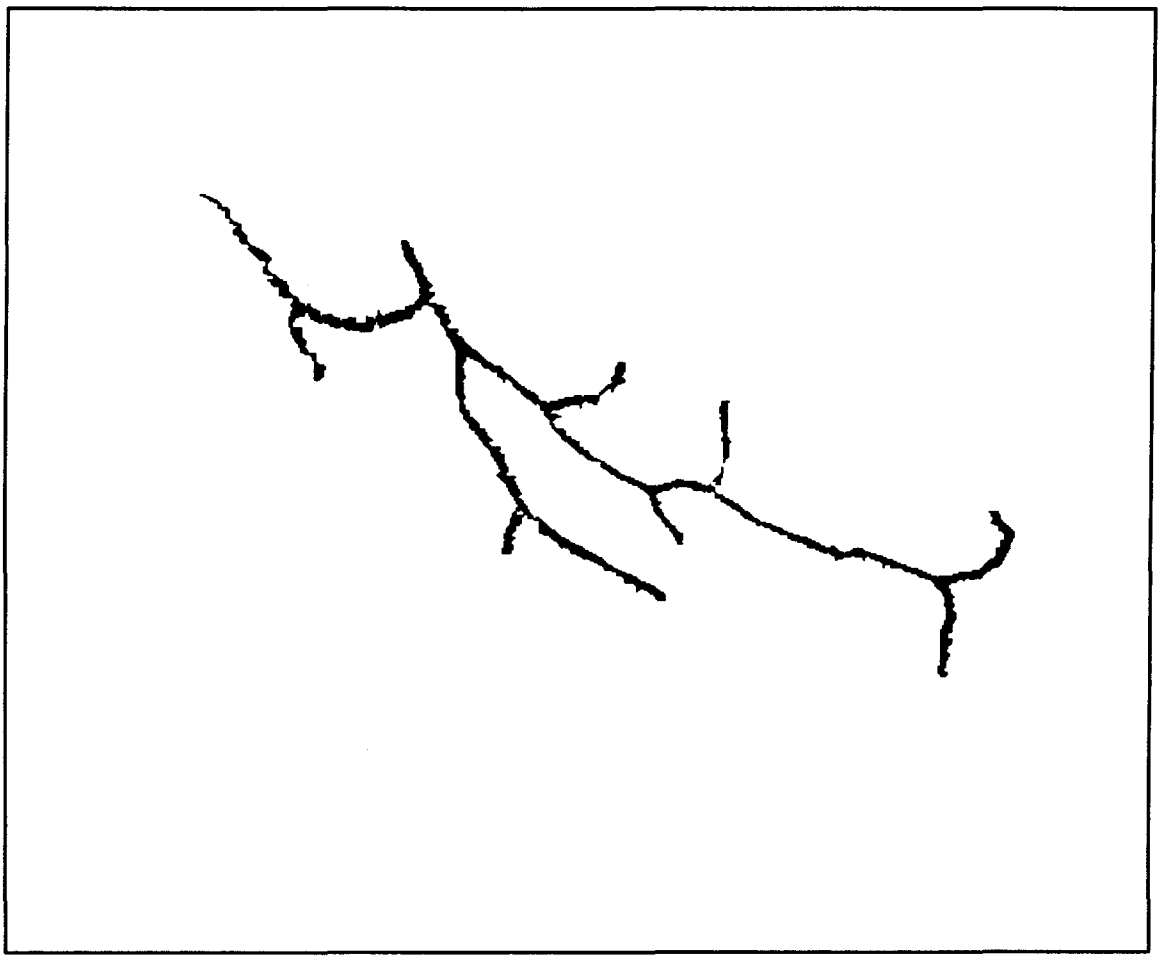

Figure 36 Segmented LDM muscle

	Level	X1	Y1	X2	Y2	L	S	A	D	T
1	A1	396	248	1000	542	862.66	671.75	8950	10.37	0.284
2	A2	946	618	954	724	116.5	106.3	1236	10.6	0.09
3	A2	658	520	684	580	72.7	65.3	606	8.33	0.11
4	A2	700	516	724	422	119.8	97.01	1039	8.66	0.23
5	A2	456	364	506	590	258.18	231.46	2782	10.77	0.11
6	A3	520	536	670	642	191.6	183.67	2196	11.46	0.04
7	A2	422	314	200	198	321.2	250.47	4026	12.5	0.282
8	A3	292	318	314	402	101.62	86.8	1047	10.3	0.17
9	A2	544	428	626	380	115.12	95.15	1239	10.7	0.211

Table 3 Results of Quantification of a complete LDM muscle

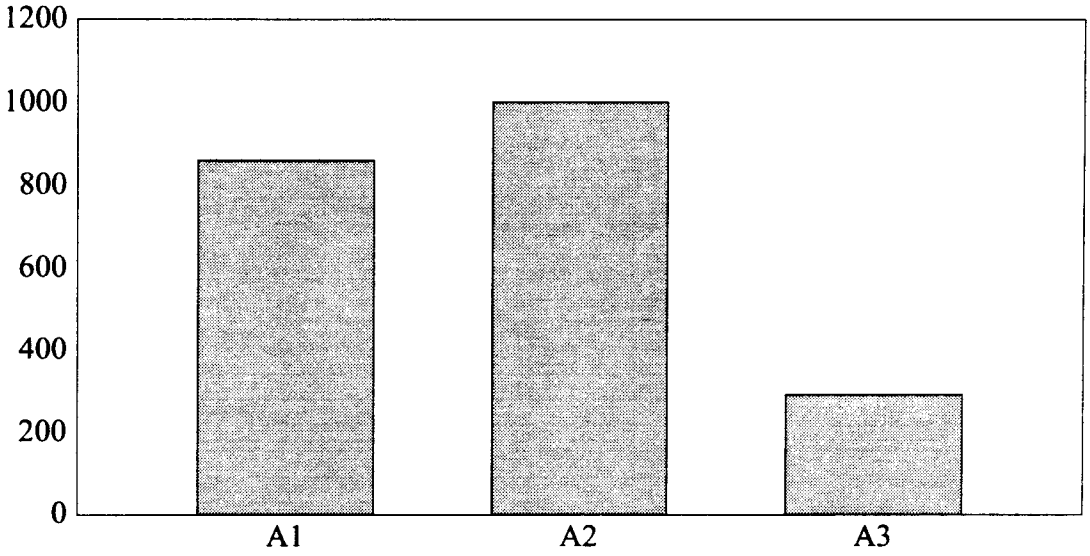

Figure 37 Histogram Distribution of the Vessel Length

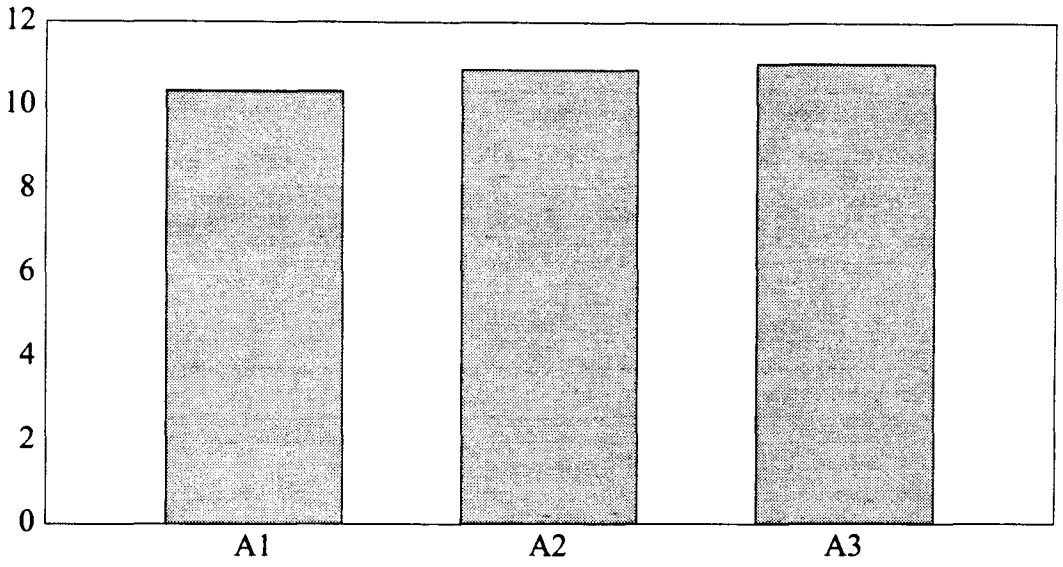

Figure 38 Histogram Distribution of the Vessel Diameter

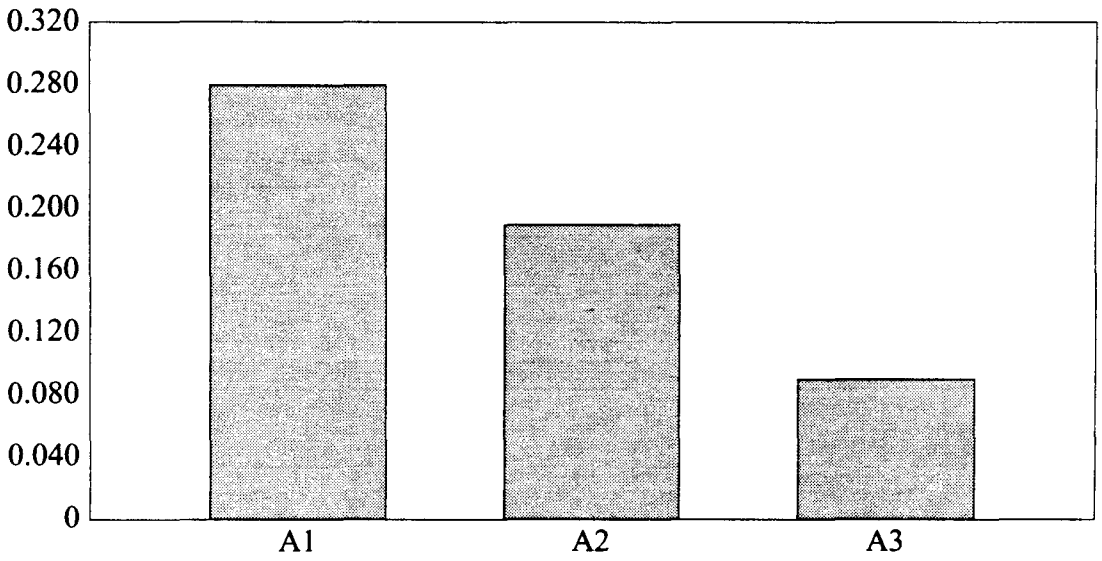

Figure 39 Histogram Distribution of the Vessel Tortuousity

CHAPTER V
DISCUSSION

A. Image Registration

In this section we discuss the registration functions experimented with, the quality of the digitized sub_images and different overlap resolution strategies that we tried.

1. Registration Functions

We have experimented with two registration functions, CBC and CC, both yielded correct results in all of or test cases. We choose the peak sharpness measure [14] as another criterion for selecting the registration method to be used. Let p be the height of the peak, q the height of the registration surface 3 pixels away from the peak location, q/p is the peak sharpness PS, with 0 indicating a perfect peak, and 1 indicates no peak at all. Table 3 lists PS values for the different tests we ran on the registration methods. The values were computed at 4 neighbor points surrounding the peak. It is clear the CBC outperforms CC under this criterion, and is considered more robust. CBC is more computationally intensive than CC, however, the robustness of the method was more important than its computational complexity, thus we chose the CBC as the method of registration.

	CBC	CC
Window 1 (216, 275)	0.62	0.76
Window 2 (350, 271)	0.64	0.33
Window 3 (402, 53)	0.62	0.65

Table 4 PS Values for Different Test Windows.

2. Digitized Sub_image Quality

The digitized sub_images were of very poor quality, presenting low contrast, and high variance inside regions of the same object. The illumination faded out as we moved away from the center of the image. Histogram Equalization was performed on the sub_images to enhance the contrast, and enable the human expert to identify the common features in the sub_images more easily .

B. Image Segmentation

In this section, we discuss the segmentation algorithm parameters, sensitivity and performance under different conditions.

1. Algorithm Parameters

The selection of the parameter W greatly affects the performance of the algorithm. In this algorithm we assume that the cross section encompasses only one vessel segment. Increasing W enables us to work on segments of the vessel with higher curvature (with wider cross sections we are sure that the edges, as well as the center line will be included in the cross section). However, with higher cross section width, we were not able to deal with thin, adjacent segments (the algorithm will, in some cases, misidentify the point P_i, and thus E_{i1}, and E_{i2}). In this work we have chosen a fixed value for W that enables us to work with the narrowest vessels of interest. We had to operate on vessels with high curvature on several stages and obtained satisfactory final results. On further work, we would like to experiment with a dynamic value of W.

2. Algorithm Sensitivity to User Input

The algorithm determines the number of cross sections, their orientation and starting location from the two points A, and B defined by the user. Orientation and number of cross sections are insensitive to the variations in A, and B. The first and last cross sections' locations are dependent on the exact location of A, and B respectively. When working with cas-

caded vessel segments, point B of one segment must coincide with point A of the next segment to ensure continuity of the detected edges.

CHAPTER VI
CONCLUSIONS AND RECOMMENDATIONS

The system developed in this thesis is to reconstruct and segment microcirculatory images, as well as obtain several morphological measurements. The system will allow researches to more precisely reconstruct the microvascular sub_images, and produce more accurate, and consistent results. Even though this system was developed for a specific project at the University of Louisville Division of Plastic and Reconstructive Surgery, it can be easily adapted and used in other medical research projects with the same nature.

The first recommendation would be to improve the quality of the microscope images which are captured and digitized. Improvements in the original sub_images would greatly enhance the resultant images, as well as enable us to exploit different registration and segmentation algorithms that were not possible to use with the current images.

The registration and segmentation algorithms needs to be further developed so as to minimize the user interaction.

The system is currently implemented in two separate modules, integrating the two modules in one seamless work environment is an essential step towards allowing non–technically oriented researchers to use the system. The Image Reconstruction module was the result of months of spiral development, the patches and mix of C/C++ present in the code would make its maintenance very hard. Re–coding this module should be the first step taken before any modification is done to that module.

REFERENCES

[1] Malpighi, Marecello: De Pulmonibus: observationes anatomical Bologna, 1661. in Selected Readings in the History of Physiology. John Fulton, ed, C.C. Thomas, Springfield, III. 1956.

[2] Leeuwenhoek, A. von: Den Waaragtigen Omloop des Bloeds, als mede dat de Arterien en Venae gecontinueerde Bloed – Vatem zijn Kloor veor de Ooegen gestelt. Verhandelt in een Brief geschreven aan de Koninglijke. Societeit tot London. 65th Missive, Sept. 7, 1688. Opuscula selecta Neerlandicorum de Arte medica. Fasc. 1:45, 1907.

[3] Rafael C. Gonzalez, and Richard E. Woods, "Digital Image Processing," 3rd ed., Addison–Wesley Publishing Company, Inc., 1993, pp 416–423

[4] Gonzalez, pp 438–443.

[5] Milan Sonka, Michael D. Winniford, and Steve M. Collins, "Robust Simultaneous Detection of Coronary Borders in Complex Images," *IEEE Trans. Med. Imag.*, vol. 14, no. 1, pp 151–161, March 1995

[6] Mário A. T. Figueirdo, José M. N. Leitão, "A Nonsmoothing Approach to the Estimation of Vessel Contours in Angiograms," *IEEE Trans. Med. Imag.*, vol. 14, no. 1,pp 162–172, March 1995

[7] Gonzalez, pg 458.

[8] Allen P. Johnson, "Development of a Computer Vision System to Detect Thrombi," M. Eng. Thesis, EMCS Dep., University of Louisville, Aug. 1990.

[9] Allen P. Johnson, "Development of a Computer Vision System to Detect Thrombi," M. Eng. Thesis, EMCS Dep., University of Louisville, Aug. 1990.

[10] R. Hummel, S. Zucker and A. Rosenfeld, "Scene Labelling by Relaxation Operations," *IEEE Trans. Syst., Man Cyber.*, vol. SMC–6, no. 6, pp 420–433, June 1976

[11] S. Peleg, "A New Probabilistic Relaxation Scheme, " *IEEE Trans. Pattern Anal. Mach. Intell.*, vol. PAMI 2, no. 4, pp 362–369, July 1980

[12] L. G. Brown, "A Survey of Registration Techniques," *ACM Computing Surveys*, vol. 24, no. 4, pp 325–376, Dec. 1992.

[13] J. Y. Chiang, and B. J. Sullivan, "Coincident Bit Counting–A New Criterion for Image Registration," *IEEE Trans. Med. Imaging*, vol. 12, no. 1, pp 30–38, March 1993.

[14] M. D. Pritt, "Automated Subpixel Image Registration of Remotely Sensed Imagery," *IBM J. Res. Develop.*, vol. 38, no. 2, pp 157–166, March 1994.

[15] Robert A. Rapson, "The Development of an Image Processing Technique to Detect Thrombi," M. Eng. Thesis, EMCS Dep., University of Louisville, Aug. 1989.

[16] Kenung Wu, David Gauthier, and Martin D. Levine, "Live Cell Segmentation," *IEEE Trans. Biomed. Eng.*, vol. 42, no. 1, pp pp 1–12, Jan 1995

[17] C. K. Chow, T. Kaneko, "Automatic Boundary Detection of the Left Ventricle from Cineangiograms," *Comp. Biomed. Res.*, vol. 5, pp 388–410, 1972.

VITA

Mohamed S. Mansour was born on May 16, 1968 in Cairo, Egypt. He graduated from As–Salam College High School in Cairo in June 1986. He entered Faculty of Engineering at Ain Shams Universsity in September 1986 and received his Bachelor of Science degree in June 1991. He will receive hs Master of Science degree in August 1995.